The Development of the Lower Extremity of a Human FE Model and the Influence of Anatomical Detailed Modelling in Vehicle-to-Pedestrian Impacts

Shouhei Kunitomi, Yoshihiro Yamamoto, Ryosuke Kato, Jacobo Antona-Makoshi, Atsuhiro Konosu, Yasuhiro Dokko, Tsuyoshi Yasuki

Abstract The goal of this study was to develop and validate a 50th percentile male pedestrian finite element model on a component-to-full scale and to clarify the influence of anatomical details in human modelling on the impacted body response and injury patterns. First, we developed a 50th percentile male Japan Automobile Manufacturers Association pedestrian model including anatomical detail, especially for the lower extremities using CT/MRI data, then we validated the model at the component/sub-assembly levels as well as the full-scale level using available post-mortem human subject impact test data. As a result, we were able to develop a highly biofidelic Japan Automobile Manufacturers Association pedestrian finite element model which can precisely predict post-mortem human subject injury patterns of the lower extremities under various impact conditions. Furthermore, focusing on the effectiveness of anatomical detailed modelling for the pelvis and knees, such as in the model developed in this study, the authors examined the influence of the modelling against body response as well as injury patterns. As a result, we found that the pelvis cortical bone thickness has a significant influence on the force deflection response as well as injury patterns of the pelvis. Furthermore, we clarified that detailed knee ligament modelling improves knee ligament injury patterns under pedestrian full-scale impact conditions.

Keywords biofidelity, human finite element models, injury, pedestrian,

I. INTRODUCTION

Lower extremities injuries (LEIs) account for more than 30% of all moderate-to-fatal injuries in vehicle-to-pedestrian impacts [1]. These injuries predominantly include long bone fractures, knee ligament injuries and pelvic fractures. Although infrequently life-threatening, LEIs are commonly associated with permanent medical impairment of substantial cost to the victims and society [2]. This situation has increased the awareness of these types of injuries as illustrated by international initiatives aiming at the prevention of pedestrian LEIs when hit by vehicles [3-4].

Numerous experimental studies with post-mortem human subjects (PMHSs) have investigated pedestrian LEI mechanisms and thresholds. These studies include component, sub-assembly and full-scale tests. Femur, tibia and fibula bone fracture mechanisms and thresholds have been investigated in bending tests with or without flesh [5-6]. Knee ligament rupture mechanisms and thresholds have been investigated in sub-assembly knee tension [7-8], lateral bending and combined lateral shear and bending [9]. Pelvic fractures and dislocations have been investigated through acetabular and iliac lateral impacts to an isolated pelvis [10]. On the full scale, body kinematics and LEIs have been investigated through the tests in which PMHSs in a standing position were struck laterally by the frontal part of commercial vehicles [11-12]. One problem associated with these experiments was that the results were largely dependent on the front design of the vehicles used in the experiments [13], which limited their applicability to develop standards applicable to all vehicles. This limitation has been recently addressed by incorporating testing methods that deliver impacts to PMHSs with a generic buck. These vehicle design independent methods have been applied to develop the corridors for standardised 50th percentile male size (M50) whole body kinematics that can be used to evaluate such physical or numerical tools as anthropomorphic test devices (ATDs) or human body computer models for pedestrian [14-16].

A pedestrian Finite Element (FE) model [17-19] is one type of research tool that has proved to be useful for

Shouhei Kunitomi (skunitomi@jari.or.jp, +81 29 856 0885), Y. Yamamoto, R. Kato, J. Antona-Makoshi and A. Konosu are Research Engineers at the Japan Automobile Research Institute (JARI) in Tsukuba, Japan. Y. Dokko and T. Yasuki are members of the Japan Automobile Manufacturers Association, Inc. (JAMA) in Tokyo, Japan.

virtual evaluation of pedestrian safety countermeasures. One of the examples of such application is that the Total Human Model for Safety (THUMS) model was used for investigating muscular and initial position effects for pedestrian kinematics and injuries [20-21]. Pedestrian FE models have also been utilised to support the development of physical testing devices such as, for example, a leg form impactor [22-23]. Overall, the effectiveness of the countermeasures and tools developed using pedestrian FE model will be influenced by its biofidelity. As medical imaging technologies evolve, computational power increases, and new PMHS data become available, the anatomical detail and the biofidelity that can be achieved by the FE models also increases. This calls for a continuous update of the models' anatomical accuracy and biofidelity. However, the previous Japan Automobile Manufacturers Association's (JAMA) pedestrian model [19] has not been updated for several years and its biofidelity, such as the knee ligament shape and the thickness distribution of the pelvis, is insufficient. In addition, the Global Human Body Models Consortium (GHBMC) model reproduces the connection between the muscle and the bone in detail, and incorporates the cortical bone thickness distribution of ribs and limb bones. GHBMC notes that they will continue enhancement of all GHBMC models [24]. Therefore, it is necessary to incorporate anatomical details into the JAMA pedestrian model in order to investigate more detailed mechanisms of pedestrian pelvis and lower limb injuries. In addition, clarifying how the details incorporated into a pedestrian FE model affect its response to impacts can contribute to the development of more effective and specific LEI preventive countermeasures.

The ultimate goal of this study was to support the development of strategies that aim to prevent LEIs in pedestrians hit by vehicles. The specific aim is twofold:

a) To present the development and component-to-full scale validation of the M50 JAMA pedestrian model that incorporates particularly detailed lower extremities, knees and hip regions.

b) To investigate how the anatomical details incorporated into the knees and pelvis of the JAMA pedestrian model affect the LEIs prediction in the simulations of pelvis impact tests and generic buck-to-PMHS experiments.

II. METHODS

The lower extremities of the M50 human JAMA pedestrian model have been developed and validated against published literature data at the component and sub-assembly levels. The validated sub-assemblies were merged with the upper body of the previous JAMA pedestrian model [19] and the full body model was then validated against full-scale PMHS impact experiments. Hereafter, this developed and validated JAMA pedestrian model is referred to as the modified JAMA pedestrian model. The lower extremities of the JAMA pedestrian model were newly created based on CT images of PMHS close to M50 (height: 175cm, weight: 78kg). Furthermore, the femur, fibula, tibia and pelvis were scaled to a standard M50 size based on anatomical dimensional data [25-26]. The connections of bone and ligament, and bone and flesh, are sharing nodes and bone-to-bone contacts are defined in the hip joint and knee joint regions. Mesh size was adjusted so that the timestep is more than 0.1 ms, in consideration of practicality. Several parts of the JAMA pedestrian model was modified in more detail based on published data, that is, attachment area and shape morphology of knee ligaments were modified and distribution of pelvic cortical bone thickness and sacral foramina were incorporated. The validation items from published data are summarised in TABLE I. The thigh and leg model were validated against dynamic 3-point bending tests [5-6][27]. The simulation results showed good correlation with the experimental results in Fig. A1-5 (Appendix A). The material properties are shown in Fig. B1-2 (Appendix B). Full scale generic buck to pedestrian impact tests were conducted using a generic buck model validated at the component level. Finally based on the modified JAMA pedestrian model, the influence of detailed modelling of the knee and pelvis in a pelvis dynamic loading impact test and full scale generic buck-to-pedestrian impact was investigated. Detailed descriptions of the knee and pelvis models and validation results are provided below and the other model validation results and properties are shown in Appendix A and B. In the present study, simulations were conducted using PAM-CRASH (ESI, Paris, France, Version 2012).

TABLE I
Validation items used for the modified JAMA pedestrian model

Part	Validation items	Reference
Thigh	Dynamic 3-point bending (Proximal third, Mid-shaft, Distal third)	[5-6]
	Dynamic 3-point bending with flesh (Mid-shaft, Distal third)	[27]
Leg	Dynamic 3-point bending (Proximal third, Mid-shaft, Distal third)	[5-6]
	Dynamic 3-point bending with flesh (Proximal third, Mid-shaft, Distal third)	[27]
Knee	Quasi-static and dynamic knee ligament tension tests	[7-8]
	standardisation of ligament shape and the attachment area	[28-44]
	knee 3, 4-point bending tests	[9] [45]
Pelvis	Pubic symphysis: compression and tension tests	[46]
	Pelvis: dynamic loading impact tests	[10]
	Hip joint: adduction and abduction characteristics tests	[47]
Whole body	Generic buck component validation	[16]
	Full scale generic buck-to-pedestrian impact	[14-15]

JAMA Pedestrian Model Development and Validation

Detailed knee model

Fig. 1 shows the detailed knee model including menisci. This model was created based on the Japan Automobile Research Institute (JARI) knee model [48], and modified by published PMHS photographs and size data [28-44]. The detailed knee model consists of medial collateral ligament (MCL), lateral collateral ligament (LCL), posterior cruciate ligament (PCL) and anterior cruciate ligament (ACL) and meniscus. The MCL ligament is a shell element, the meniscus is a hexa element, the LCL, PCL and ACL ligaments are modelled with hexa elements and bar elements. By using a hexa element for the LCL, PCL, and ACL, these models can reproduce the complicated ligament shape and the attachment area with the bone. In addition, the biofidelity of the model was improved by dividing the PCL into A-PCL/P-PCL and the ACL into A-ACL/P-ACL from anatomical literature [49]. Comparison of the ACL and PCL attachment areas with experimental data [28-41] is shown in Fig. A7 (Appendix A). As a result, the ACL and PCL models showed a good match with experimental attachment areas.

Fig. B3 (Appendix B) shows the quasi-static stress-strain curve for the knee ligament bar and shell models. These stress-strain curves, ultimate stress and ultimate strain values were applied by referring to the literature [50-54]. Since the main role of the hexa element is contact, its material properties were determined to be softer than the bar element so as to have little influence on the knee ligament tension characteristics. The dynamic properties of knee ligament models were determined by the tuning force-deflection response against a dynamic knee ligament tension experiment [7-8]. The meniscus property was applied by referring [55] in Fig. B4 (Appendix B).

The detailed knee model was validated against quasi-static and dynamic knee ligament tension tests [7-8] and knee 3 and 4-point bending tests with PMHSs [9][45]. Descriptions of the knee 4-point bending test is provided below and the other test validation results are shown in Fig. A6 and A8 (Appendix A). The simulation model representing the dynamic knee 4-point bending test is shown in Fig. 2. In the test, the knee cut to the prescribed size was fixed to a potting cup, and the bending force was applied to the knee by ram at two loading points.

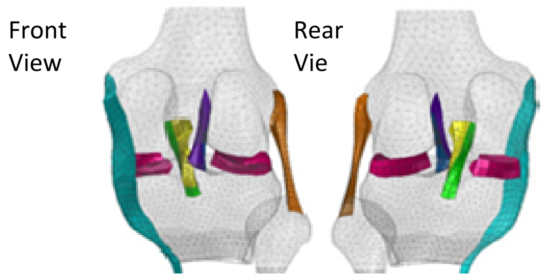

Fig. 1. Detailed knee model.

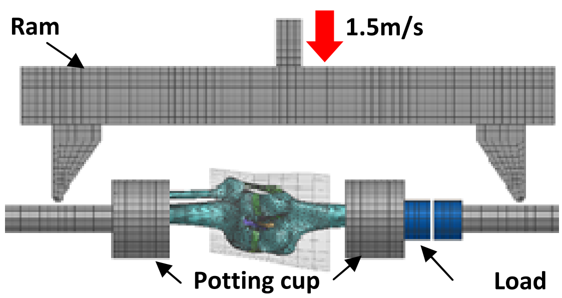

Fig. 2. Knee 4-point bending simulation setup [9].

Detailed pelvis model

The geometry of the detailed pelvis model was modelled by CT images from PMHSs. In addition, Kato's method [56] which automatically extracts the cortical bone thickness from CT images and reflects it on the images was adopted which was reflected on the FE model. Therefore, by setting actual cortical bone thickness for each shell element, a detailed ilium model was made possible (Fig. 3) and the CT images used for the pelvis model were selected from PMHSs of height and weight close to M50. Fractures along the sacral wing and sacral foramina occurred both in the real world [57] and the pelvis experiment [10]. For the purpose of accurately reproducing the sacral injuries, the sacrum model created detailed parts such as the sacral foramina and the sacral canal using CT images. The detailed pelvis model modelled cortical bone as a shell element and cancellous bone as a tetra element.

Fig. 4 and 5 show the sacroiliac ligament, pubic symphysis and acetabulum models. These models were modelled by a hexa element. The sacroiliac joint model consisted of two models: the interosseous sacroiliac ligament, which is a strong short ligament filling the gap between the rough surface of the ilium and the sacrum, and the articular cavity which is located in front of the interosseous sacroiliac ligament which inside is filled with synovial fluid. The pubic symphysis model was modelled to fill the space based on the boundary between the iliac bones in the CT images. In the acetabulum model, the thickness of the acetabulum was adjusted so that the width from the femoral head was 1 mm, and a contact was set against the femoral head.

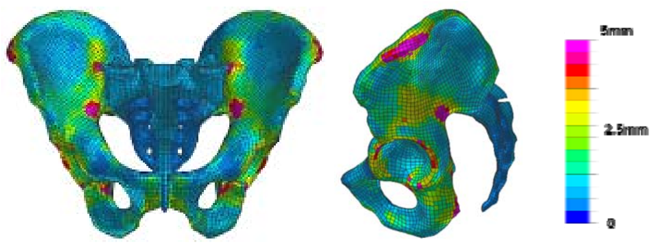

Fig. 3. Pelvis detailed model (thickness distribution of cortical bone).

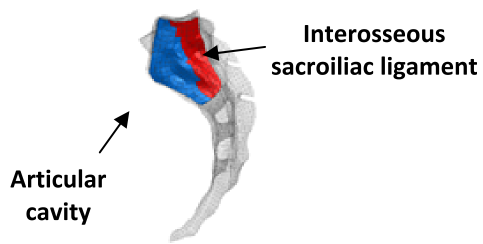

Fig. 4. Sacroiliac ligament model: side view.

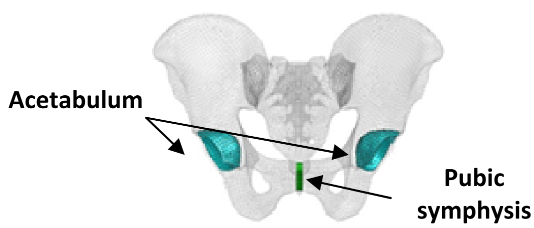

Fig. 5. Pubic symphysis and acetabulum model.

Material properties of the pelvis cortical bone were validated from pelvis impact test data [10] within the published values of the iliac coupon test [58]. Because of the lack of data for the cancellous bone of the ilium and sacrum, the material properties were defined based on literature of the femur cancellous bone [59-61]. Likewise, due to the lack of data for material properties of the interosseous sacroiliac ligament and the joint cavity, these properties were determined by the tuning force-deflection response of a pelvis impact test [10]. In this pelvis impact test, dislocation of the sacroiliac joint occurs. Dislocation is a state in which the ligament, cartilage, and bone are damaged, and the bones constituting the joint lose the correct positional relationship. In order to reproduce this dislocation with the pelvis model, ultimate strain was defined for the interosseous sacroiliac ligament model and the joint cavity model. Pubic symphysis material properties were tuned by pubic symphysis compression and tension test data [46]. By using MAT 45 (PAM-CRASH), material properties of compression and tension are defined. However, due to the restrictions of MAT 45, the ultimate strain cannot be set individually. Therefore, the reduction of the force in the tension test is expressed by lowering the stress in the high strain region of the tension characteristic. Acetabulum material properties were applied by referring to (elastic module:1.20MPa, Poisson’s ratio:0.46) [62-63]. These material properties are shown in Fig. B5 to B7(Appendix B).

The detailed pelvis model was validated against pubic symphysis compression and tension tests [46] and pelvis dynamic loading impact tests [10]. Descriptions of the pelvis impact test are provided below and pubic symphysis compression and tension test results are shown in Figure A9 (Appendix A). In the pelvis impact test, half of the pelvis was fixed with two potting cups, and the loads were measured just under the cups. Loads were applied to either the iliac wing or the acetabulum, and in order to measure the two loads on the acetabulum and iliac load cells individually, the contralateral side of the pelvis was cut along a line defined from the mid distance of the two anterior iliac spines and the top of the greater sciatic notch. Fig. 6 shows the pelvic impact test model and the outline of the experiment.

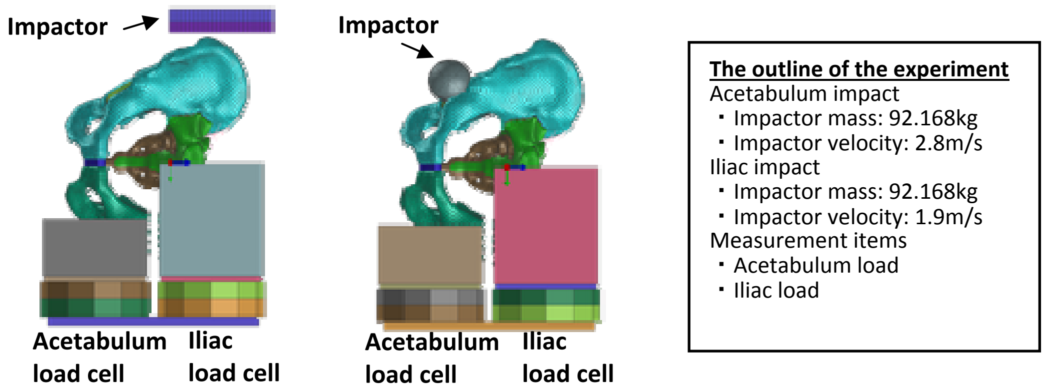

Fig. 6. Pelvis model validation simulation setup [10].

Modified JAMA pedestrian model

The modified JAMA pedestrian model is shown in Fig. 7. Based on the previous JAMA pedestrian model [19], the modified JAMA pedestrian model was validated and its lower extremities were developed. The number of nodes is approximately 200,000, and the number of elements approximately 650,000. TABLE II is shown main modification points for the modified JAMA pedestrian model.

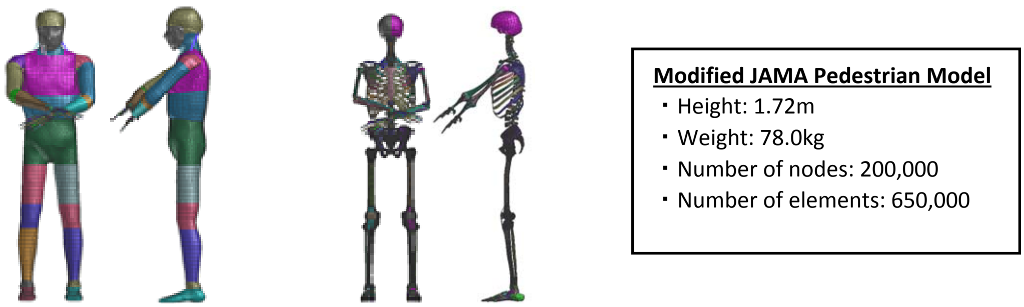

Fig. 7. The modified JAMA pedestrian model.

TABLE II
Main modification points for the modified JAMA pedestrian model

Part	Modification points	Reference
Thigh	Incorporation of JAMA knee model (distal femur)	[48]
	Changing material property of flesh	[64-65]
Leg	Incorporation of JAMA knee model (proximal tibia)	[48]
	Changing material property of flesh	[64-65]
Knee	Incorporation of JAMA knee model (knee ligaments)	[48]
	standardisation of ligament shape and the attachment area	[28-44]
	Changing material properties of knee ligaments and meniscus	[7-9] [45] [50-55]
Pelvis	Modelling new geometry from CT images	
	Incorporation of detailed cortical bone thickness distribution	[56]
	Changing material properties (Bone, Pubic symphysis, etc.)	[10] [46-47] [58-61]

Full scale generic buck-to-pedestrian impact

The modified JAMA pedestrian model with enhanced biofidelity was validated against full scale generic buck to pedestrian impacts tests [14-15]. Fig. 8 shows the simulation model representing the full scale generic buck to pedestrian impacts tests and the outline of the experiment. The initial posture of the PMHS was adjusted targeting the positioning guidelines described in [66]. Therefore, the initial posture of the modified JAMA pedestrian model was determined based on the size and photographs of the PMHS given in the literature[14]. The generic buck model was created referring to the dimensional data, mass data, material characteristics and photographs of literature, and each parts was validated against experimental data [16]. The modified JAMA pedestrian model was evaluated in a lateral generic buck impact at 40km/h.

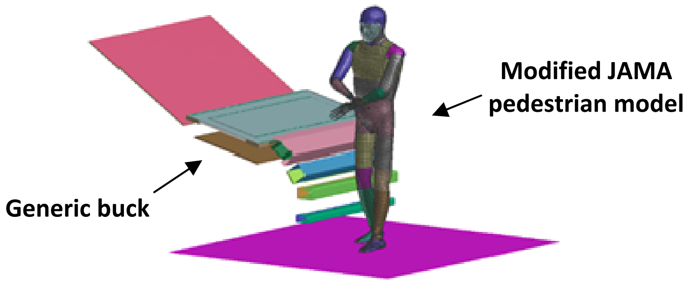

The outline of the experiment
- Impact direction: Lateral
- Buck velocity: 40 km/h
- Measurement items: PMHS trajectory and injuries, Buck interaction force

Fig. 8. Full scale generic buck to pedestrian impact simulation setup [14-15].

Simulation model for the influence of detailed modelling

The influence of detailed modelling was confirmed by pelvis dynamic loading impact tests [10] and full scale generic buck-to-pedestrian impact tests [14-15]. TABLE III describes the simulation matrix for confirming the influence of detailed modelling.

In the pelvis dynamic loading impact test, the influence of a detailed sacrum structure and pelvis cortical bone thickness was investigated. The content of the comparison is the force-deflection response and injury pattern. The Case 1 pelvis model is the modified JAMA pedestrian pelvis model. The Case 2 model was created by filling sacral foramina and sacral canal holes of the Case 1 pelvis model (Fig. 9a). The Case 3 model has the average cortical bone thickness of the Case 1 pelvis model (Fig. 9b). The average cortical bone thickness is 1.24mm.

In the full scale generic buck-to-pedestrian impact tests, the influence of the knee ligament modelling method and pelvis cortical bone thickness was investigated. The comparison included stress/strain distribution and injury pattern. The Case 4 model is the modified JAMA pedestrian model. Case 5 is a model in which the knee ligament of the Case 4 model was replaced with the previous JAMA pedestrian knee ligament model made by a shell element [19] (Fig. 9c). The Case 6 model uses the average thickness of the pelvis model (Case 3 model).

TABLE III Simulation matrix for confirming the influence of detailed modelling

Case No.	Type	Test method	Change point from modified JAMA pedestrian model
1	Component	Pelvis dynamic loading impact	None (modified JAMA pedestrian pelvis model)
2	Component	Pelvis dynamic loading impact	Filling sacral foramina and sacral canal holes
3	Component	Pelvis dynamic loading impact	Averaging pelvis cortical bone thickness
4	Full scale	Generic buck-to-pedestrian impacts	None (modified JAMA pedestrian model)
5	Full scale	Generic buck-to-pedestrian impacts	Replacing with the previous knee ligaments
6	Full scale	Generic buck-to-pedestrian impacts	Averaging pelvis cortical bone thickness

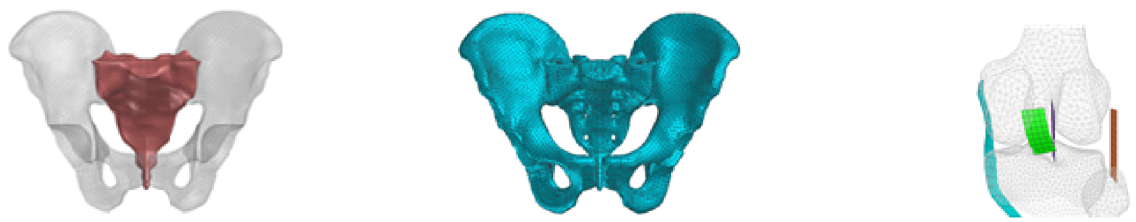

a) Filling sacral foramina and sacral canal holes (Case 2)
b) Averaging pelvis cortical bone thickness (Case 3, 6)
c) Replacing with the previous knee ligament model (Case 5)

Fig. 9. Models comparing the influence of detailed modelling.

III. RESULTS

JAMA Pedestrian Model Validation

Detailed knee model

The knee 4-point bending models were validated against the moment-angle corridors developed by [45] based on the results of the dynamic knee 4-point bending tests [9]. The simulation results (red) showed good correlation with the experimental corridor (blue) in Fig. 10. The MCL model fracture occurred at 13.5 degrees, which is the same result as the experimental PMHS result in Fig. 11 and Table AI (Appendix A).

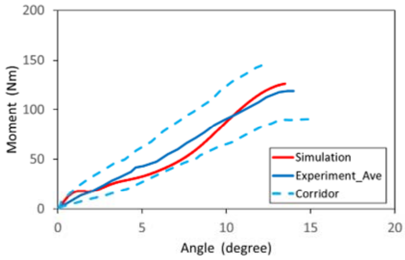

Fig. 10. Moment-angle response for knee 4-point bending test [9][45].

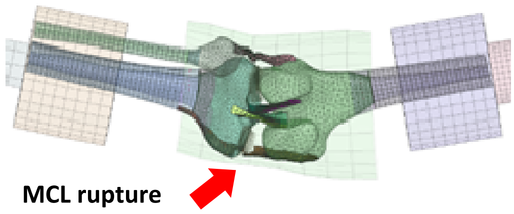

Fig. 11. Knee 4-point bending simulation result.

Detailed pelvis model

Fig. 12 shows the validation corridor [67] and detailed pelvis model simulation results of the pelvic impact test [10]. From this figure, the simulation result shows good force response characteristics to the pelvic impact validation corridor. Fig. 13 shows the strain distribution in the cancellous bone of the pelvis impact test. In iliac loading, dislocation of the sacroiliac joint occurred. Initially, strain was applied to the ilium, and, as the strain increases, the deviation between the ilium and the sacrum increased. Finally, the sacroiliac joint was dislocated. Numerous dislocations of the sacroiliac joints were also observed in the PMHS test (Table AIII: Appendix A), so this prediction closely matched the results of the experiment. In acetabulum loading, bone fractures occurred in order of superior pubic ramus on the struck side, superior pubic ramus on the opposite side, inferior pubic ramus on the struck side, and finally sacral ala along the sacral holes. These injuries were reproduced well in the PMHS results (Table AIV: Appendix A).

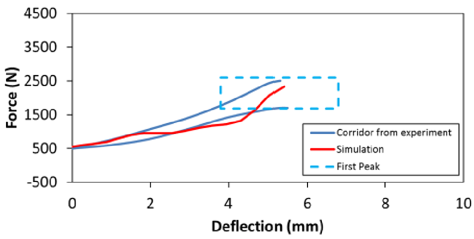

a) Iliac force in iliac impact

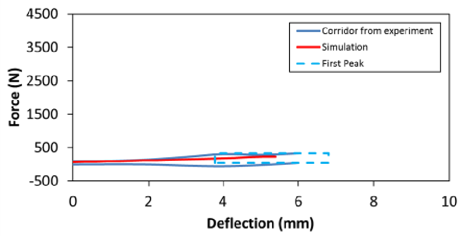

b) Acetabulum force in iliac impact

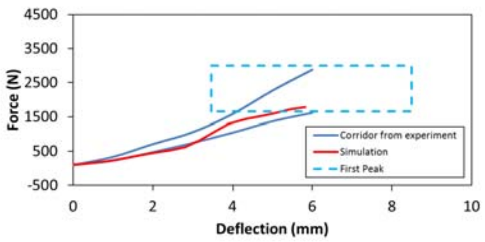

c) Iliac force in acetabulum impact

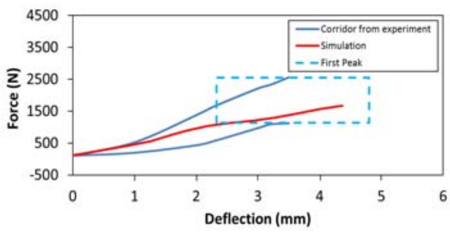

d) Acetabulum force in acetabulum impact

Fig. 12. Force-deflection response for pelvis impact test [67].

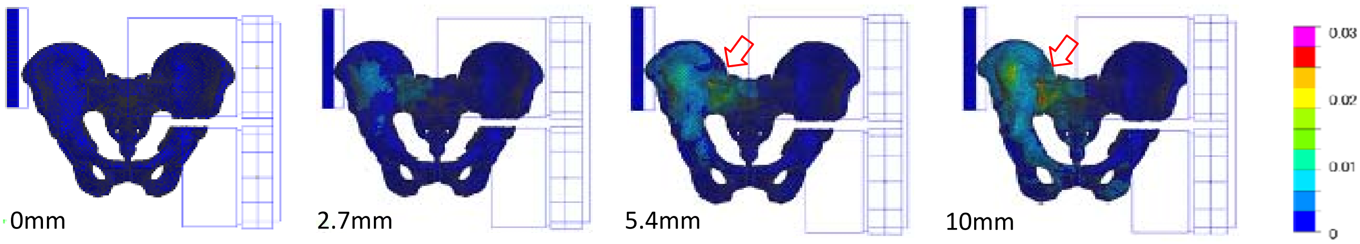

a) Simulation injury result in iliac impact
Dislocation

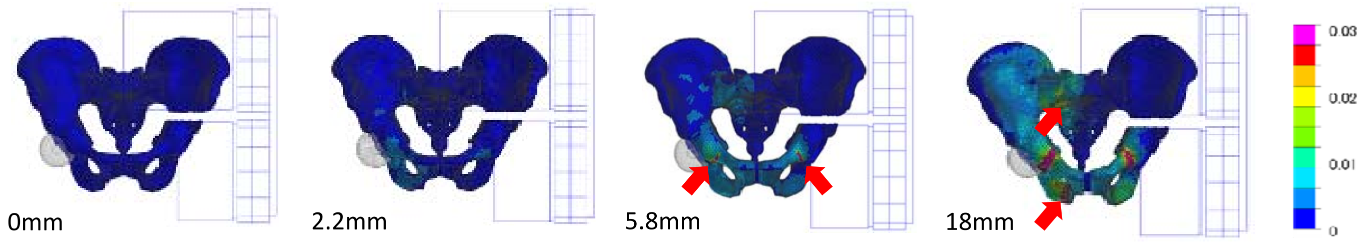

b) Simulation injury result in acetabulum impact
Fracture point

Fig. 13. Strain distribution in the cancellous bone of the pelvis impact test.

Full scale generic buck-to-pedestrian impact

Fig. A12 shows a comparison of whole-body kinematics (side view) of PMHS test and simulation results [15]. In the modified JAMA pedestrian model, after the upper bumper of the vehicle model collides with the right knee, the entire right leg begins to curve along the grille and bumper around the knee. At 45ms, the pelvis initiates contact in a posture that sits on the hood edge. After that, the leg begins to separate from the vehicle, and the upper body starts to rotate around the pelvis. At 90ms, the leg completely detaches from the vehicle, and in the upper body the head maintains its initial posture due to the side bending of the neck, but the other parts rotate. After 90ms, the legs are on the hood, the shoulder touches the windshield and the head starts to rotate around the shoulder. Then, at 140ms, the head collides with the windshield. This series of kinematics was also observed in the PMHS experiments. The trajectory of each part (Head, T1, T8, Pelvis) of the modified JAMA pedestrian model is within the corridor of the PMHS test results [14] in Fig. 14. Table IV summarises the results of the injuries of the full scale generic buck to pedestrian impact tests [15]. In PMHSs, rib fracture, pelvic injury, knee ligament rupture, and spinal fracture mainly occurred. The simulation result using the modified JAMA pedestrian model also shows similar injuries (pelvis and rib fracture, right MCL and left LCL rupture). Therefore, it can be concluded that the modified JAMA pedestrian model kinematics in the full scale generic buck to pedestrian impacts test showed generally good agreement with those of the actual test.

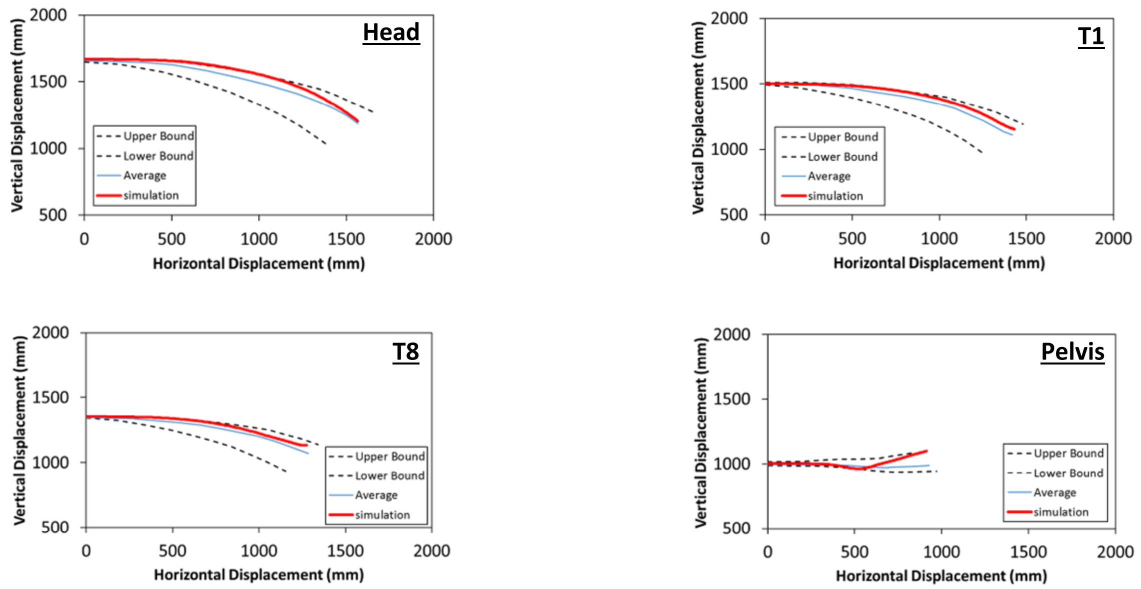

Fig. 14. Trajectory of each part (Head, T1, T8, Pelvis) of the modified JAMA pedestrian model [14].

TABLE IV Results of the injuries of the full scale generic buck to pedestrian impact test [15]

Part	PMHS 1 (V2370)	PMHS 2 (V2371)	PMHS 3 (V2374)	Modified JAMA Pedestrian model
Pelvis	No injury	No injury	R,L: Pubic ramus R,L: Sacral ala	R: Pubic ramus
Knee	lateral retinaculum	R: MCL , L: LCL	R: MCL, ACL , L: LCL	R: MCL , L: LCL
The others	Rib: R2~3, L1, L10~12 Cervical Spine	Rib: R2, R4~7, L1, L10~12, Cervical Spine	Rib: R1~5, L2~5, L9~10 Cervical Spine	Rib: R1~5, R11~12, L1, L10~12

Results for influence of the detailed model

Pelvis dynamic loading impact test

TABLE V lists the results of the injuries of the pelvis dynamic loading impact simulation. In iliac impact, dislocation of the sacroiliac joint occurred in all models. However, in acetabulum impact, the sacrum fracture pattern showed different results among the models. Fig. 15 compares the strain distribution in the sacrum cancellous bone of the acetabulum impact test at the end of simulation (18mm). From this figure, high strain occurs in the sacral holes in the Case 1 model and along the sacroiliac joint in Case 2. Also, bone fractures occurred in these high strain regions.

As shown in Fig. 16, averaging the pelvis cortical bone thickness (Case 3) has a large influence on the force deflection response. In both impacts, Case 3 iliac force was lower than the other models. In acetabulum impact, a delay occurred until the first peak in Case 3. In addition, in Case 2, the iliac force rose more quickly than in Case 1 in both impact simulations. It seems that the force from the impactor to each iliac load cell became easier to transmit by filling the sacral foramina and canal holes in Case 2. A quantitative evaluation was carried out by CORA [68] for these models. As a result, the superiority of the detailed model was shown in the evaluation. The CORA rating values of each model are as follows: (Case 1: 0.795, Case 2: 0.781, Case 3: 0.646)

Fig. 17 shows strain distribution in the pelvis cancellous bone in the acetabulum impact at each first peak. Therefore, it was found that these first peaks were caused by superior pubic ramus fracture. These results indicate that anatomical details of the pelvis model affect the prediction of injury pattern and force-deflection response in lateral pelvis impact.

TABLE V Result of the injuries of the pelvis dynamic loading impact simulation

Impact point	Case1	Case2	Case3
Iliac	R: Dislocation of sacroiliac joint	R: Dislocation of sacroiliac joint	R: Dislocation of sacroiliac joint
Acetabulum	R: superior/inferior pubic ramus, Fracture along the sacral holes L: superior pubic ramus	R: superior/inferior pubic ramus, Fracture along the sacroiliac joint L: superior pubic ramus	R: superior/inferior pubic ramus, L: superior pubic ramus

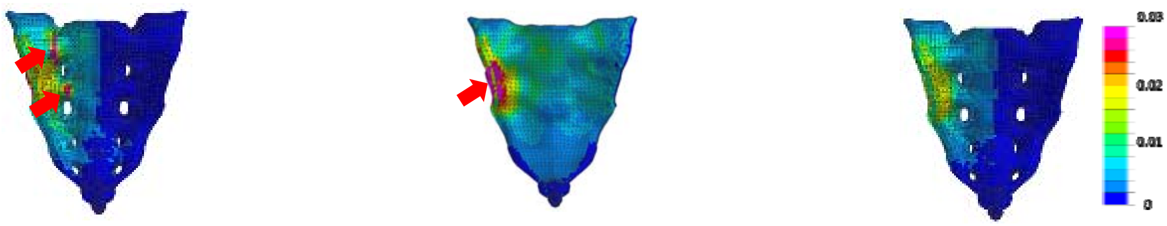

a) Case 1 sacrum model b) Case 2 sacrum model c) Case 3 sacrum model

Fig. 15. Strain distribution in the sacrum cancellous bone. Fracture point

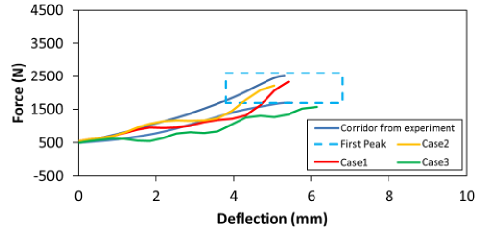

a) Iliac force in iliac impact

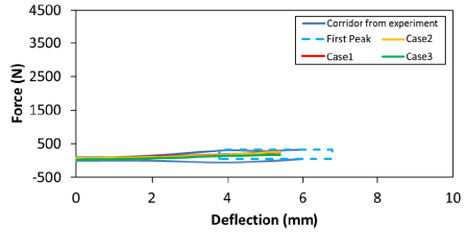

b) Acetabulum force in iliac impact

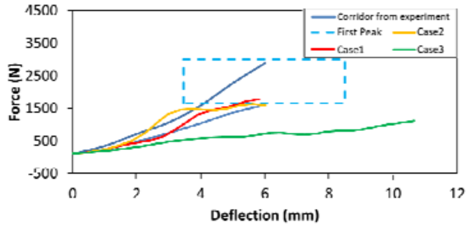

c) Iliac force in acetabulum impact

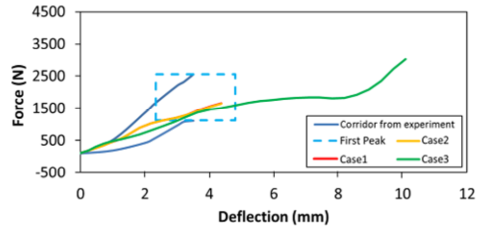

d) Acetabulum force in acetabulum impact

Fig. 16. Force-deflection response for the pelvis dynamic loading impact test [67].

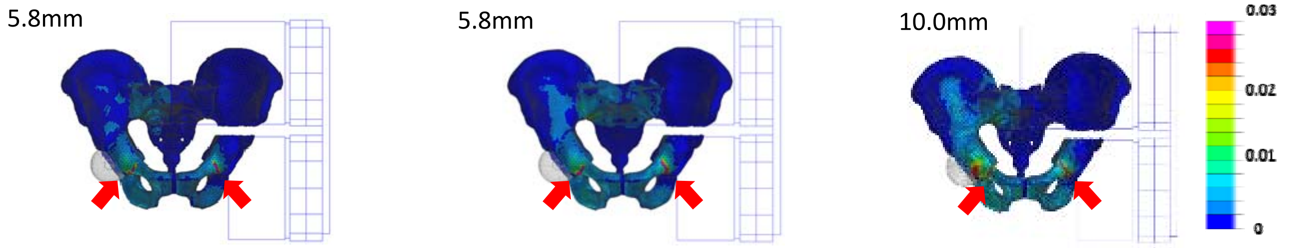

a) Case 1 sacrum model b) Case 2 sacrum model c) Case 3 sacrum model

Fig. 17. Strain distribution in pelvis cancellous bone in acetabulum impact. Fracture point

Full scale generic buck-to-pedestrian impacts test

TABLE VI lists the results of the injuries of full scale generic buck to pedestrian impact simulation. In Case 5, the injuries of the knee ligament increased, and in Case 6, a pubic ramus fracture did not occur.

TABLE VI
Result of the injuries of the full scale generic buck to pedestrian impact simulation

Part	Case 4	Case 5	Case 6
Pelvis	R: Pubic ramus	R: Pubic ramus	None
Knee	R: MCL, L: LCL	R: MCL,LCL,PCL, L: LCL,ACL	R: MCL, L: LCL
The others	Rib: R1～R5,R11,R12 L1,L10-12	Rib: R1～R5,R11,R12 L1,L10-12	Rib: R1～R6,R11,R12 L1,L10-12

Influence of knee ligament modelling method (comparison of Case 4 and Case 5)

In a comparison study between Case 4 and Case 5, there was a difference in the injuries of the knee ligament. In Case 4, the right MCL and left LCL were ruptured, whereas rupture occurred in right MCL, right/left LCL, right PCL and left ACL in Case 5. Fig. 18 shows a comparison of the knee ligament behaviour of Case 4 and Case 5 on the right leg (struck side) showing particularly different injuries. First, knee bending occurred due to collision of the leg and the bumper of the generic buck. This led to an MCL extension and rupture (0~23ms). Next, the leg separated from the bumper, and contact between the thigh and the grill started. Because the thigh was pushed in the impact direction, bending and shearing occurred simultaneously in the knee joint. At 57ms, the Case 5 PCL model was ruptured. Last, bending in the opposite direction occurred in the knee joint by striking up the leg. As a result, the Case 5 LCL model was lengthened and ruptured. Fig. 19 shows comparison of the PCL ligament stress distribution. In the Case 5 PCL model, stress was generated by shearing of the knee and ruptured at 57ms. However, almost no stress was generated in the Case 4 PCL model. From these results, the difference in stress distribution between Case 4 and Case 5 became clear.

a) Case 4 model: knee ligament behaviour

b) Case 5 model: knee ligament behaviour

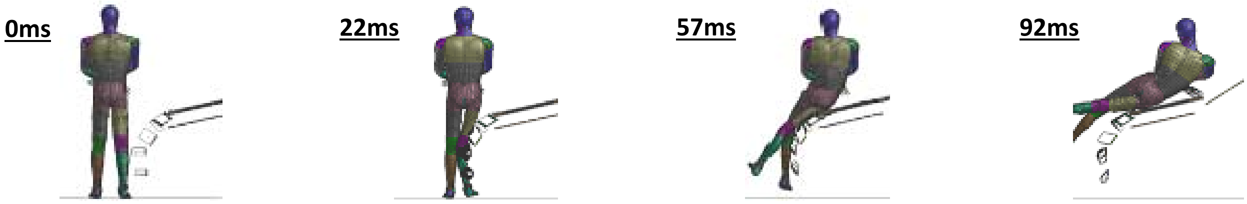

c) Case 4 model: full body behaviour

Fig. 18. Comparison of the knee ligament behaviour of Case 4 and Case 5.

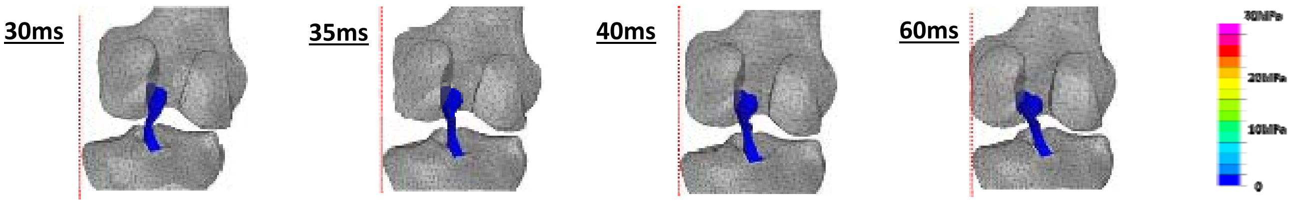

a) Case 4 model: PCL ligament model

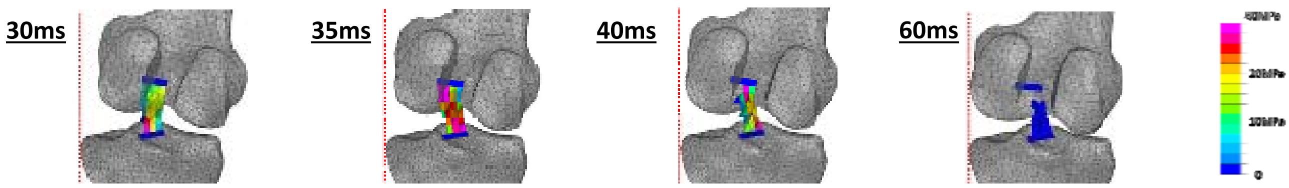

b) Case 5 model: PCL ligament model

Fig. 19. Comparison of the PCL ligament stress distribution.

Influence of pelvis cortical bone thickness (comparison of Case 4 and Case 6)

In the Case 4 and Case 6 models, there was a difference in fracture of the iliac bone. Fig. 20 shows the strain distribution in the cancellous bone of the pelvis at 50ms. In Case 6, strain around the acetabulum was high due to the impact load through the femoral head, and no fracture occurred. On the other hand, in Case 4, bone fracture occurred in the struck side superior pubic ramus area where the iliac cortical bone thickness is thin.

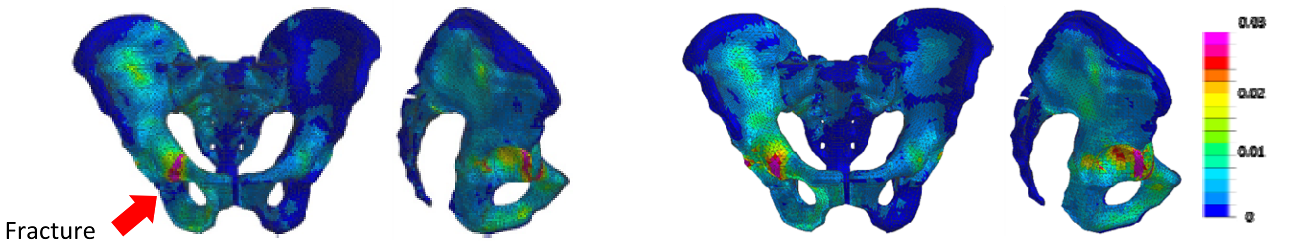

a) Case 4 pelvis model b) Case 6 pelvis model

Fig. 20. Strain distribution in pelvis cancellous bone.

Fracture point

IV. DISCUSSION

The lower extremities of the previous M50 JAMA pedestrian model [19] were developed and validated in published literature data on component-to-full scale. The ilium, sacrum and knee joints models were modelled more precisely than the previous JAMA pedestrian model, and sacroiliac joints, acetabulum, etc. were newly incorporated. As a result, the modified JAMA pedestrian model accurately reproduced injury patterns such as bone fractures along the sacral holes and rupture of the knee ligament in lateral impact tests, and was able to obtain good agreement with the experiments.

The influence of implementation of the anatomical details into the pelvis and knee to simulate precise body response and injury patterns was clarified in a pelvis dynamic loading impact test and full scale generic buck impact.

In the pelvis dynamic loading impact test, anatomical details of the pelvis model affected the prediction of injury patterns and force-deflection responses. In the injury pattern of acetabular impact, high strain was generated around the sacral holes in the Case 1 model which led to fracture along the sacral holes, but it did not occur in the other models (Fig. 15). In Case 2, because the sacral holes are filled, stress concentration did not occur around the sacral holes, and fractures occurred along the sacroiliac joint. Although the Case 3 model reproduced the sacral holes in detail, the stiffness around the sacral holes increased and fractures did not occur due to the averaging of the cortical bone thickness. This indicates that the detailed structure of the sacrum and appropriate cortical bone thickness setting generated stress concentrations around the sacral holes, and reproduced the PMHS injury patterns. In the force-deflection response, the cortical bone thickness has a great influence. Especially at the acetabulum impact of Case 3, the iliac force against the displacement decreased, and each first peak was delayed as compared with other models (Fig. 16). One of the factors of the force reduction is that the stiffness of the ilium decreased because the Case 3 iliac bone thickness (1.24mm) was thinner than the average thickness of the iliac bone of Case 1 (1.53mm). On the other hand, the acetabulum force increased because the cortical bone thickness around the pubic ramus increased. Moreover, stress concentration was alleviated by averaging, and local bone fracture in the pubic ramus became less likely to occur compared to the Case 1 model. This is one reason why the first peak was delayed. In previous studies of pelvic lateral loading impact [69-74], the cortical bone thickness of the pubic ramus is thinner than other parts and stress concentration and fractures around the pubic ramus occurred frequently. Furthermore, it was found that changes to cortical bone thickness had the largest effect on cortical bone strains [75]. These results indicate that an anatomical detailed pelvis model is important for analysis of injury patterns and force-deflection response in lateral pelvis impact. In this case, the cortical bone thickness distribution has more influence on injury patterns and force-deflection responses than a local structure such as sacral holes, so the cortical bone thickness distribution should be preferentially incorporated into the model.

In full scale generic buck impact, the anatomical details of the knee ligament model revealed that it is important for the injury patterns of the knee ligaments. A detailed knee ligament model consists of bar elements and hexa elements. A bar element reproduces the tensile characteristics of the ligament using a tension only bar, and a hexa element plays a role of contact. Therefore, the detailed model generated little stress due to compression and shear, and it was possible to reproduce flexibility of the knee ligament accurately. On the other hand, in the Case 5 knee ligament model, since the constituent shell element retained its in-plane shape, stress was generated against the movement in the shearing direction of the knee, and the ligament ruptures (Fig. 19). Reference [18] also indicated that shell elements generate compressive stress, which may result in unrealistic knee behaviour. In addition, the knee ligaments using the shell element and the solid element caused serious local concentration of the ligament deformation, leading to low failure strain [76]. Therefore, these explanations agree with our study. On the other hand, the detailed modelling of the cortical bone thickness of the iliac affects the fracture pattern of the pelvis. In the averaged thickness model, no fracture occurred and strain around the acetabulum was high. In the pelvic detailed model, since the cortical bone thickness of the ilium was precisely reproduced, stress concentration occurred at the thin area and the pubic ramus fractures (Fig. 20). It is found that a pubic rami fracture occurs by distributing the load that pass through the femur head and 61.5 % of the pedestrian pelvic fractures include fracture of the pubic ramus [77]. And it is revealed that approximately 60% of pedestrians whose pelvis was broken had pubic ramus fractures on the struck side [78]. Therefore, the literature indicates that the probability of pubic ramus fractures on the struck side occuring is high and are identical to our simulation results. In full scale generic buck impact, not only the thickness distribution but also the anatomical details of the knee ligament model showed a high influence on the injury patterns and stress distribution of the knee ligaments and their importance was indicated. This study suggests that it is vital to implement anatomically details in a human pedestrian model, including precise structure, appropriate modelling method and material properties in order to accurately represent body kinematics and injuries in vehicle-to-pedestrian collisions.

In this study, the authors developed and validated the JAMA pedestrian model using experiments under various loading conditions. The modified JAMA pedestrian model was modelled from CT images of a PMHS close to a M50, and the posture was determined with reference to [66]. However in the real-world, pedestrians have various characteristics such as age, posture, height, gender and muscle activity. In order to predict all pedestrian injuries in various real-world situations, it is necessary to confirm the individual influences of these diversities and to develop models that allow for each characteristic.

The modified JAMA pedestrian model reproduced the structure of the human body in detail as much as possible from the CT and MRI images, and applied the properties from literature. However, a few material properties such as the interosseous sacroiliac ligament and articular cavity were determined to match the PMHS dynamic test responses, because of the lack of data from the literature. In addition, living body and PMHS differ in muscle tension and tissue condition, etc., which may cause differences in characteristics. In this study, characteristics of major parts such as bone are considered difficult to change, so loads and fractures suffered by pedestrians can be accurately predicted from experimental results using PMHS. Clarifying how the details incorporated into a pedestrian FE model affect its response to impacts can lead to more effective and appropriate injury prediction and contribute to LEI preventive countermeasures. In order to more accurately predict pedestrian tissue level injuries, experiments using volunteers and well preserved PMHS are necessary. If these material property data can be obtained in the future, those characters can be updated.

V. CONCLUSIONS

The modified JAMA pedestrian FE model with the lower extremities of a M50 human was developed from medical images and was validated based on data from literature. The influence of implementation of the anatomical details into the pelvis and knee to simulate precise body response and injury patterns in impacts was clarified. In the pelvis, it was found that the cortical bone thickness had a great influence on the force deflection response and generation of the stress concentration. Further, by modelling the detailed structure, it became possible to reproduce complicated injury patterns such as the sacrum fracture. In the knee ligaments, it was shown that the result of injury changed by modelling element type and ligaments structure. These results highlight the importance of anatomical details in human modelling on body response and lower extremity injury patterns in vehicle-to-pedestrian impacts.

VI. REFERENCES

[1] Mizuno, Y. Summary of IHRA pedestrian safety WG activities proposed test methods to evaluate pedestrian protection afforded by passenger cars. Proceedings of 18nd ESV Conference, 2003, Nagoya, Japan.

[2] L. Blincoe, A. Seay, E. Zaloshnja, T..Miller, E. Romano, S.Luchter, R.Spicer. The economic impact of motor vehicle crashes 2000. NHTSA Technical Report, 2002.

[3] Global Road Safety Partnership, Global technical regulation. Internet: http://www.unece.org/trans/main/wp29/wp29wgs/wp29gen/wp29glob_registry.html, accessed 21 February 2017.

[4] European Enhanced Vehicle-safety Committee. EEVC Working Group 17 Report Improved test methods to evaluate pedestrian protection afforded by passenger cars, EEVC, 1998.

[5] Kerrigan, J R, Bhalla, K S, Madeley, N J, Funk, J R, Bose, D, Crandall, J R. Experiments for Establishing Pedestrian-Impact Lower Limb Injury Criteria. Proceedings of SAE Conference, paper no. 2003-01-0895, 2003, Detroit, USA.

[6] Kerrigan J R, Drinkwater D C. Tolerance of the human leg and thigh in dynamic latero-medial bending. International Journal of Crashworthiness, 2004, Vol.9, No.6, p.607-623.

[7] Bose, D, Sanghavi, P, Kerrigan, J, Madeley, N, Bhalla, K, Crandall, J. Material Characterization of Ligament using Non-Contact Strain Measurement and Digitization. International Workshop on Human Subject for Biomechanical Research, 2002.

[8] van Dommelen, J, Ivarsson, B, Characterization of the Rate-Dependent Mechanical Properties and Failure of Human Knee Ligament. Proceedings of SAE Conference, paper no. 2005-01-0293, 2005, Detroit, USA.

[9] Bose, D, Bhalla, K, Rooij, L, Millington, S, Studley, A, Crandall, J. Response of the Knee Joint to the Pedestrian Impact Loading Environment. Proceedings of SAE Conference, paper no. 2004-01-1608, 2004, Detroit, USA.

[10] Salzar, R S, Genovese, D, Bass C R, Bolton, J R, Guillemot, H, Damon, A M, Crandall, J R. Load Path Distribution within the Pelvic Structure under Lateral Loading. International Crashworthiness Conference, 14(1): 99-110, 2008.

[11] Schroeder, G, Fukuyama, K, Yamazaki, K, Kamiji, K, Yasuki, T. Injury mechanism of pedestrians impact test with a sport-utility vehicle and mini-van. Proceedings of IRCOBI Conference, 2008, Bern, Switzerland.

[12] Subit, DQ, Kerrigan, J, Crandall, JR, Fukuyama, K, Yamazaki, K, Kamiji, K, Yasuki, T. Pedestrian-vehicle interaction kinematics and injury analysis of four full scale tests. Proceedings of IRCOBI Conference, 2008, Bern, Switzerland.

[13] Han, Y., Yang, J., Mizuno, K., Matsui, Y. Effects of vehicle impact velocity, vehicle front-end shapes on pedestrian injury risk. Traffic injury prevention, 13(5): 507-518, 2012.

[14] Forman, J L, Joodaki, H, Forghani, A, Riley, P, Bollapragada, V, Lessley, D, Overby, B, Heltzel, S, Crandall, J. Biofidelity corridors for whole-body pedestrian impact with a generic buck. Proceedings of IRCOBI Conference, IRC-15-49, 2015, Lyon, France.

[15] Forman J L, Hamed Joodaki, et al. Whole-body Response for Pedestrian Impact with a Generic Sedan Buck. Stapp Car Crash Jornal, Vol. 59, pp.401-444, November 2015.

[16] Pipkorn, B, Forsberg, C, Takahashi, Y, Ikeda, M, Fredriksson, R, Svensson, C, Thesleff, A. Development and Component Validation of a Generic Vehicle Front Buck for Pedestrian Impact Evaluation. Proceedings of IRCOBI Conference, IRC-14-82, 2014, Berlin, Germany.

[17] Yasuki T, Yamamae Y. Validation of kinematics and lower extremity injuries estimated by Total Human Model for Safety in SUV to pedestrian impact test. Journal of Biomechanical Science and Engineering, 2010, 5:340–356.

[18] Takahashi, Y, Asanuma, H, Yanaoka, H. Development of a Full-Body Human FE Model for Pedestrian Crash Reconstructions. Proceedings of IRCOBI Conference, 2015, Lyon, France.

[19] Takayama, S, Yamamoto, Y, et al. The Clarification of Individual Injury Mechanism Difference in Pedestrian FE Model Utilizing Cadaver Scaling and Posturing Techniques. Proceedings of 22nd ESV Conference, 2011, Washington DC, USA.

[20] Iwamoto, M, Nakahira, Y. A Preliminary Study to Investigate Muscular Effects for Pedestrian Kinematics and injuries Using Active THUMS. Proceedings of IRCOBI Conference, 2014, Berlin, Germany.

[21] Chen, H, Poulard, D, Crandall, J, Panzer, M. Pedestrian Response with Different Initial Positions During Simulated Impact with a Mid-Sized Sedan. Proceedings of 24nd ESV Conference, 2015, Gothenburg, Sweden.

[22] Isshiki, T, Konosu, A, Takahashi, Y. Development of an Appropriate Pedestrian Legform Impact Test Method which can be used for all Types of Vehicles including High Bumper Vehicles Development of a Simplified Upper Body Part (SUBP) FE Model. Proceedings of IRCOBI Conference, 2014, Berlin, Germany.

[23] Isshiki, T, Konosu, A, Takahashi, Y. Analysis of the Causes of Differences in Impact Responses between a Human Lower Limb and the Flexible Pedestrian Legform Impactor under Low and High Bumper Vehicle Impact Situations. Proceedings of IRCOBI Conference, 2015, Lyon, France.

[24] GHBMC, Status of the GHBMC Project. Internet: http://www.ghbmc.com/status-of-the-ghbmc-project/, accessed 30 May 2017.

[25] Schneider L. W. Development of anthropometrically based design specifications for an advanced adult anthropomorphic dummy family, volume 1. final report, 1983.

[26] Reynolds, H. M., Snow, C. C., & Young, J. W. Spatial geometry of the human pelvis. FEDERAL AVIATION ADMINISTRATION OKLAHOMA CITY OK CIVIL AEROMEDICAL INST, 1982.

[27] Ivarsson, J, Lessley, D, Dynamic Response Corridors of the Human Thigh and Leg in Non-Midpoint Three-Point Bending. Proceedings of SAE Conference, paper no. 2005-01-0305, 2005, Detroit, USA.

[28] Girgis F G, Marshall J L, Monajem A, The cruciate ligaments of the knee joint. Anatomical, functional and experimental analysis. Clinical Orthopaedics and Related Research, 106:216–231, 1975.

[29] Odensten M, Gillquist J. Functional anatomy of the anterior cruciate ligament and a rationale for reconstruction. The Journal of Bone & Joint Surgery, 1985, Am 67:257–262.

[30] Staubli H U, Rauschning W. Tibial attachment area of the anterior cruciate ligament in the extended knee position. Anatomy and cryosections in vitro complemented by magnetic resonance arthrography in vivo. Knee Surg Sports Traumatol Arthrosc, 2:138‐ 146, 1994.

[31] Morgan C D, Kalman V R, Grawl D M. Definitive landmarks for reproducible tibial tunnel placement in anterior cruciate ligament reconstruction. The Journal of Arthroscopic and Related Surgery, 1995, 11:275–288.

[32] Muneta T, Takakuda K, Yamamoto H. Intercondylar notch width and its relation to the configuration and cross-sectional area of the anterior cruciate ligament. A cadaveric knee study. The American Journal of Sports Medicine, 1997, 25:69–72.

[33] Cuomo P, Edwards A, Giron F, Validation of the 65 degrees Howell guide for anterior cruciate ligament reconstruction. The Journal of Arthroscopic and Related Surgery, 2006, 22:70–75.

[34] Colombet P, Robinson J, Christel P, Morphology of anterior cruciate ligament attachments for anatomic reconstruction a cadaveric dissection and radiographic study. The Journal of Arthroscopic and Related Surgery, 2006, 22:984–992.

[35] Edwards A, Bull A M, Amis A A. The attachments of the anteromedial and posterolateral fibre bundles of the anterior cruciate ligament. Knee Surg Sports Traumatol Arthroscopy, 15:1414–1421, 2007.

[36] Heming J F, Rand J, Steiner M E. Anatomical limitations of transtibial drilling in anterior cruciate ligament reconstruction. The American Journal of Sports Medicine, 2007, 35:1708–1715.

[37] Siebold R, Ellert T, Metz S, et al. Femoral insertions of the anteromedial and posterolateral bundles of the anterior cruciate ligament. The Journal of Arthroscopic and Related Surgery, 2008, 24:585–592.

[38] Tallay A, Lim M H, Bartlett J. Anatomical study of the human anterior cruciate ligament stump's tibial insertion footprint. Knee Surg Sports Traumatol Arthroscopy, 16:741–746, 2008.

[39] Ferretti M, Ekdahl M, Shen W, Osseous landmarks of the femoral attachment of the anterior cruciate ligament. The Journal of Arthroscopic and Related Surgery, 2007, 23:1218–1225.

[40] Gali J C, Posterior cruciate ligament's tibial insertions: topographic anatomy and morphometric study. Revista Brasileira de Ortopedia, 48(3):263-267, 2013.

[41] Amis A A, Gupte C M, Bull A M J, Edwards A. Anatomy of the posterior cruciate ligament and the meniscofemoral ligaments. Knee Surg Sports Traumatol Arthrosc, 14:257-263, 2006.

[42] F H Fu, C F van Eck, S Tashman, J J Irrgang, M S Moreland. Anatomic anterior cruciate ligament reconstruction a changing paradigm. Knee Surgery, Sports Traumatology, Arthroscopy, Volume 23, Issue 3, pp 70–648, 2015.

[43] T Zantop, W Petersen, F H Fu. Anatomy of the anterior cruciate ligament. Operative Techniques in Orthopaedics, Volume 15, Issue 1, Pages 20–28, 2005

[44] Kopf, S., Musahl, V., Tashman, S. A systematic review of the femoral origin and tibial insertion morphology of ACL. Knee Surg Sports Traumatol Arthrosc, 17: 213, 2009.

[45] Ivarsson, J, Lessley, D, Dynamic Response Corridors and injury thresholds of the pedestrian lower extremities. Proceedings of IRCOBI Conference, September 2004, Austria.

[46] Dakin G J, Arbelaez R A, Molz F J, Alonso J E, Mann K A. and Eberhardt, A.W. Elastic and Viscoelastic Properties of the Human Pubic Symphysis Joint Effects of Lateral Impact Loading. Journal of Biomechanical Engineering, 2001, Vol. 123, pp. 218-226.

[47] National Institute of Technology and Evaluation, Human Characteristics Database. Internet: http://www.tech.nite.go.jp/human/jp/contents/cindex/database.html, accessed 1 February 2017.

[48] Takayama S, Ejima S. Investigation of Ligament Damages in Knee Bending for Traffic Accident. Journal of the Visualization Society of Japan 30(118), 2010, 25-25.

[49] Kanamori A, The anterior cruciate ligament reconstruction. Japanese Journal of Diagnostic Imaging, 2007, Vol.27, No.5, p.570-582.

[50] Pioletti D O, Rakotomanana L R, Benvenuti J F, Leyvraz P F. Viscoelastic constitutive law in large deformations application to human knee ligaments and tendons. Journal of Biomechanics, 1998, Vol.31, pp.753-757.

[51] Butler D L, Kay M D, Stouffer D C, Comparison of material properties in fascicle-bone units from human patellar tendon and knee ligaments. Journal of Biomechanics, 1986, 19.

[52] Noyes F R, Grood E S, The strength of the anterior cruciate ligament in humans and rhesus monkeys. Journal of Bone and Joint Surgery, 1976, 58-A.

[53] Race A, Amis A A, Mechanical properties of the two bundles of the human posterior crucial ligament. Journal of Biomechanical Engineering, 1994, 27.

[54] Kennedy J C, Tension studies of human knee joint ligaments, Journal of Bone and Joint Surgery, 1976, 58-A, .
[55] Yasura K, Mizuno Y, Estimation of the Mechanical Property of Meniscus Using Ultrasound Examinations of Native Meniscus and Effects of Enzymatic Digestion. Journal of Orthopaedic Reseach, 2007.
[56] Kato, R, Yamamoto, Y, Ejima, S, A methodology to develop rib finite element models that account for cortical bone thickness. Proceedings of JSAE Conference, No.39-14, 2014, Yokohama, Japan.
[57] Young JW, Burgess AR, Brumback RJ, Poka A. Pelvic fractures value of plain radiography in early assessment and management. Radiology, 160:445–451, 1986.
[58] Kemper A R, McNally C, Duma S M. Dynamic Tensile Material Properties of Human Pelvic Cortical Bone. Biomedical Science Instrumentation, 44:417-418, 2008.
[59] Martens M, The mechanical characteristics of cancellous bone at the upper femoral region. Journal of Biomechanics, 1983, 16.
[60] Brown T D, Ferguson A B. Mechanical property distributions in the cancellous bone of the human proximal femur. Journal of Acta Orthopaedica Scandinavica, 1982, 51.
[61] Lindahl O, Mechanical properties of dried defatted spongy bone. Journal of Acta Orthopaedica Scandinavica, 47, 1976.
[62] Athanasiou K A, Biomechanical properties of hip cartilage in experimental animal models. Clinical Orthopaedics and Related Research 316: 254-266, 1995.
[63] Magnussen R A, Guilak F, Vail T P. Cartilage degeneration in post-collapse cases of osteonecrosis of the human femoral head Altered mechanical properties in tension, compression, and shear. Journal of Orthopaedic Research, 2005, 23: 576-583.
[64] McElhaney, J H, Dynamic response of bone and muscle tissue. Journal of Applied Physiology, 1966, 21.
[65] Morrow, D, Tammy, L, Gregory, M, Kenton, R. Transversely isotropic tensile material properties of skeletal muscle tissue. J.Mech. Behavior of Biomechanical materials, 2009.
[66] Performance Specifications for a Midsize Male Pedestrian Research Dummy. SURFACE VEHICLE INFORMATION REPORT, J2782, October 2010.
[67] Ikeda, M, Suzuki, S, Gunji, Y, Takahashi, Y, Motozawa, Y, Hitosugi, M. Development of an Advanced Finite Element Model for a Pedestrian Pelvis. Proceedings of 22nd ESV Conference, 2011, Washington DC, USA.
[68]] Gehre, C, Gades, H, Wernicke, P. OBJECTIVE RATING OF SIGNALS USING TEST AND SIMULATION RESPONSES. Proceedings of 21nd ESV Conference, 2009, Stuttgart, Germany.
[69] Snedeker J G, Muser M H, Walz F H. Assessment of pelvis and upper leg injury risk in car-pedestrian collisions: comparison of accident statistics, impactor tests and a human body finite element model. Stapp Car Crash Jornal, Vol. 47, pp.437-457, October 2003.
[70] Untaroiu, C D, Salzar, R S, Guillemot, H, Crandall, J R. The strain distribution and force transmission path through pubic rami during lateral pelvic impacts. Proceedings of ASME 2008 International Mechanical Engineering Congress and Exposition, 2008, New York, USA.
[71] Konosu, A. Development of a Biofidelic Human Pelvic FE-Model with Several Modifications onto a Commercial Use Model for Lateral Loading Conditions. Proceedings of SAE Conference, paper no. 2003-01-0163, 2003, Detroit, USA.
[72] Ko, C, Konosu, A, Sakamoto, J, Yukita, Y. A Study on Development of a Human Pelvis FE Model by Applying in-vivo CT Information of the Human Coxal Bone. Proceedings of SAE Conference, paper no. 2006-01-0463, 2006, Detroit, USA.
[73] Anderson A E, Peters C L, Tuttle B D, Weiss J A. Development and validation of a finite element model of the pelvis. Proceedings of ASME 2003 International Mechanical Engineering Congress and Exposition, 2008, Washington DC, USA.
[74] Guillemot, H, Got, C, Besnault, B, Lavaste, F, Robin, S, Le Coz, J Y, Lassau, J. Pelvic behavior in side collisions: static and dynamic tests on isolated pelvic bones. Proceedings of 16nd ESV Conference, 1998, Windsor, Canada.
[75] Anderson A E, Peters C L, Tuttle B D, Weiss J A. Subject-Specific Finite Element Model of the Pelvis: Development, Validation and Sensitivity Studies. Journal of Biomechanical Engineering, 2005, Vol. 127, pp. 364-373.
[76] Mo, F, Arnoux, P J, Cesari, D, Masson, C. The failure modelling of knee ligaments in the finite element model. International Journal of Crashworthiness, 2012, 17:6, 630-636.
[77] Edwards, K, Green, J. Analysis of the inter-relationship of pedestrian leg and pelvic injuries. Proceedings of IRCOBI, 1999, Sitges, Spain.

[78] Ashton, S. Factors Associated With Pelvic and Knee Injuries in Pedestrians Struck by the Fronts of Cars. Proceedings of SAE Conference, Warrendale, paper no.1981-811026, 1981.
[79] Dokko, Y, Ito, O, Ohashi, K. Development of a Full‐Body Human FE Model for Pedestrian Crash Reconstructions. Proceedings of SAE Conference, paper no. 2009-01-0396, 2009, Detroit, USA.
[80] Yamada H. Strength of Biological Materials. The Williams & Wilkins Company, 1973.
[81] Nahum A M, Melvin J W. Accident Injury Biomechanics and Prevention. Springer New York, 2002.
[82] Bartleby.com. "Henry Gray (1825–1861). Anatomy of the Human Body. 1918." Internet: http://www.bartleby.com/107/indextn9.html, accessed 2 February 2017.
[83] Hewitt J, Guilak F, Glisson F, T Parker Vail. Regional material properties of the human hip joint capsule ligaments. Journal of Orthopaedic Research, 2001, 19, 359-364.
[84] J Castaing, Anatomie fonctionnelle de l'appareil locomoteur. pages 8-9, Vigot, 1977.

VII. APPENDIX A

Thigh model validation result

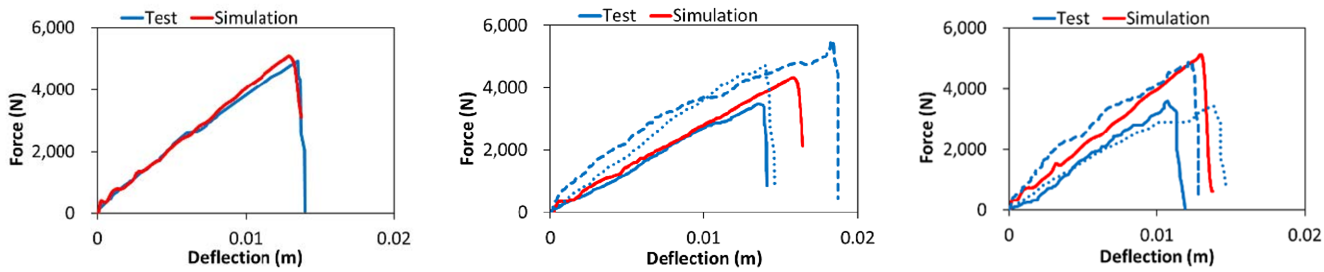

a) Proximal third b) Mid-shaft c) Distal third

Fig. A1. Femur dynamic 3-point bending [5].

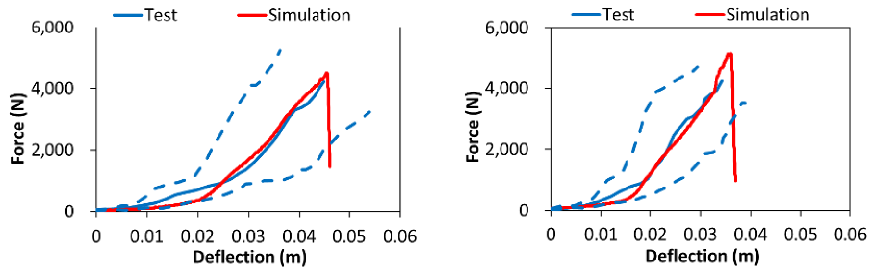

a) Mid-shaft b) Distal third

Fig. A2. Femur dynamic 3-point bending with flesh [6][27].

Leg model validation result

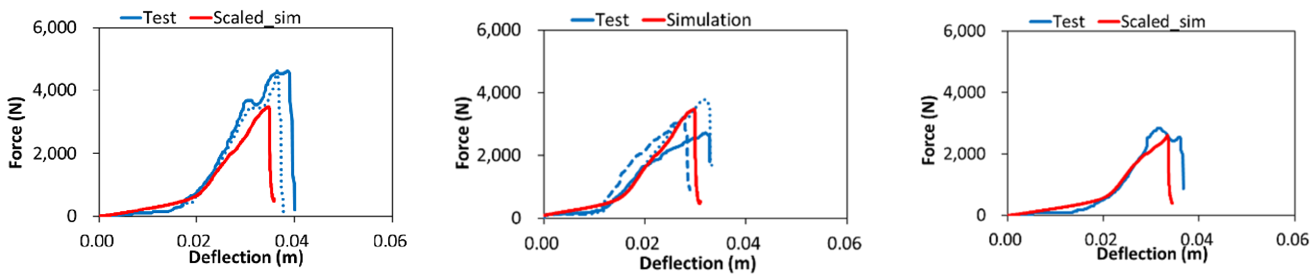

a) Proximal third b) Mid-shaft c) Distal third

Fig. A3. Tibia dynamic 3-point bending [5].

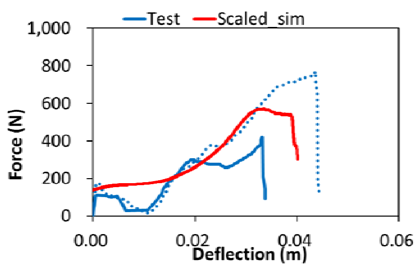

a) Proximal third

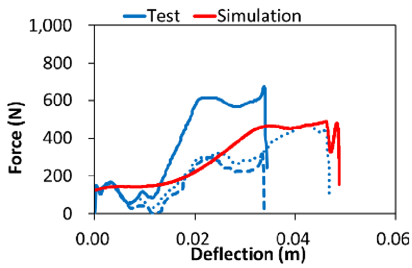

b) Mid-shaft

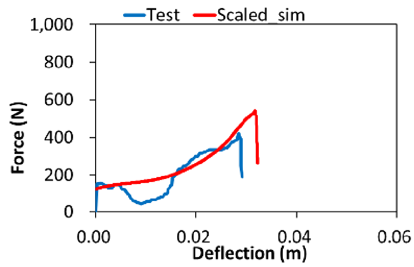

c) Distal third

Fig. A4. Fibula dynamic 3-point bending [5].

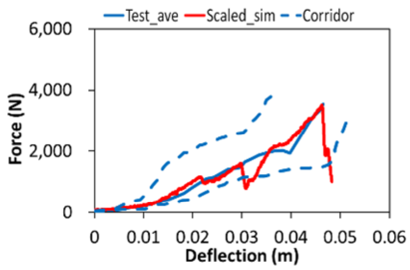

a) Proximal third

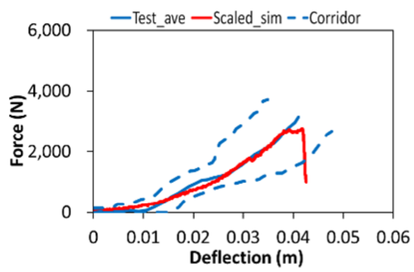

b) Mid-shaft

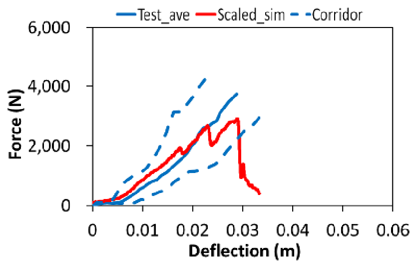

c) Distal third

Fig. A5. Leg dynamic 3-point bending with flesh [6][27].

Knee model validation result

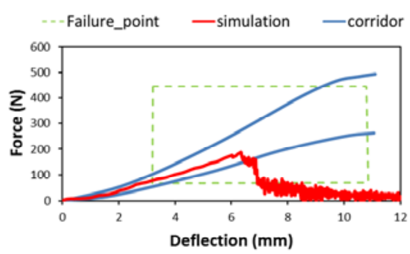

a) A_ACL 0.016 m/s

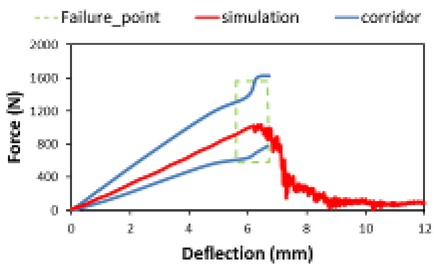

b) A_ACL 1600 mm/s

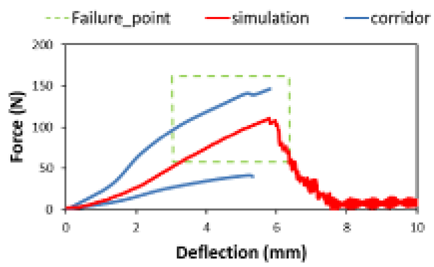

c) P_ACL 0.016 mm/s

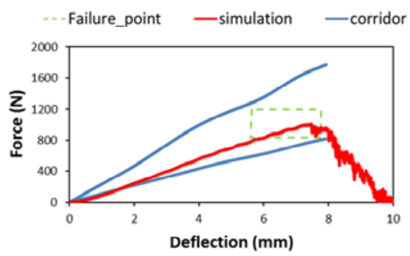

d) P_ACL 1600 mm/s

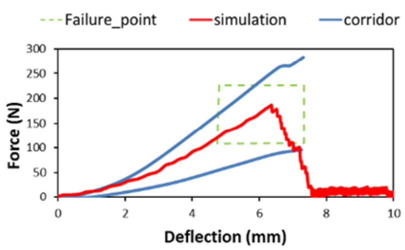

e) A_PCL 0.016 mm/s

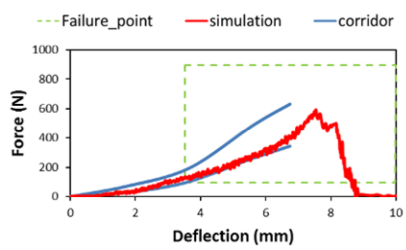

f) A_PCL 1600 mm/s

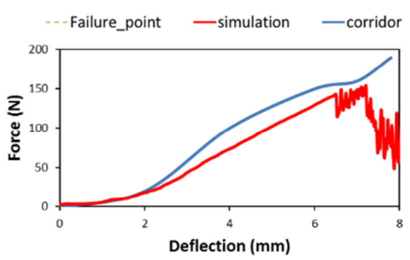

g) P_PCL 0.016 mm/s

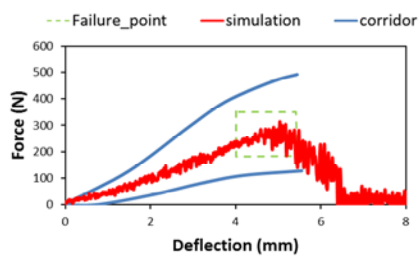

h) P_PCL 1600 mm/s

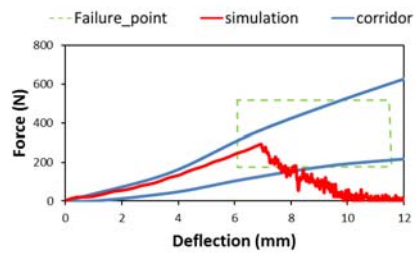

i) LCL 0.016 mm/s

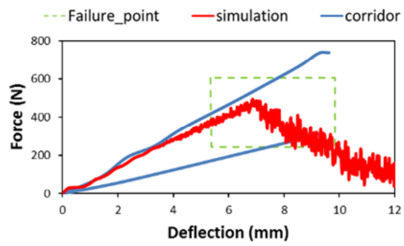

j) LCL 1600 mm/s

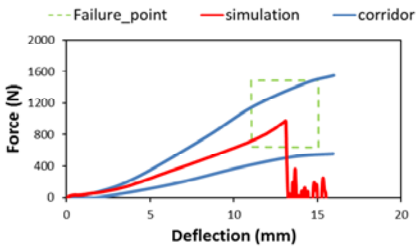

k) MCL 0.016 mm/s

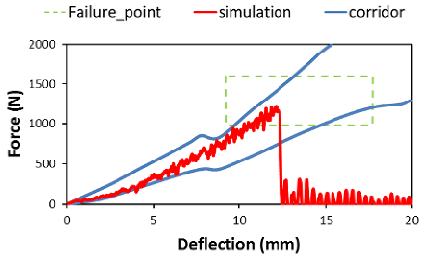

l) MCL 1600 mm/s

Fig. A6. Quasi-static & dynamic knee ligament tension test [7-8].

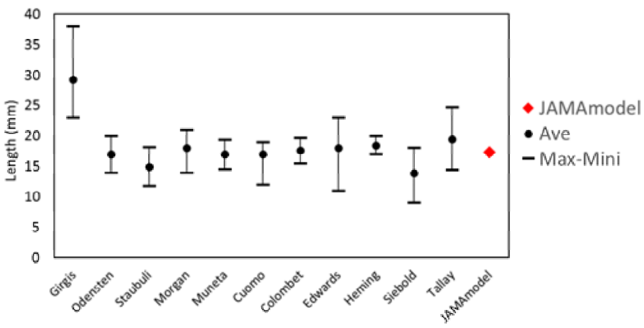

a) Length measurement of the ACL tibial insertion

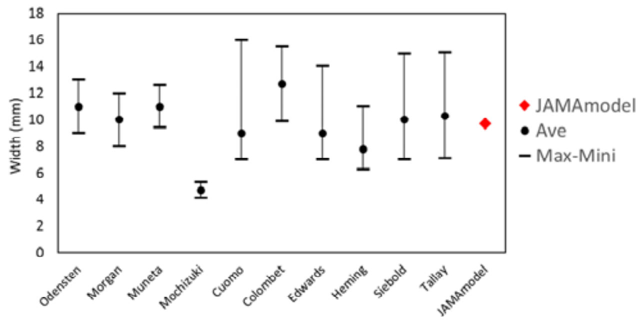

b) Width measurement of the ACL tibial insertion

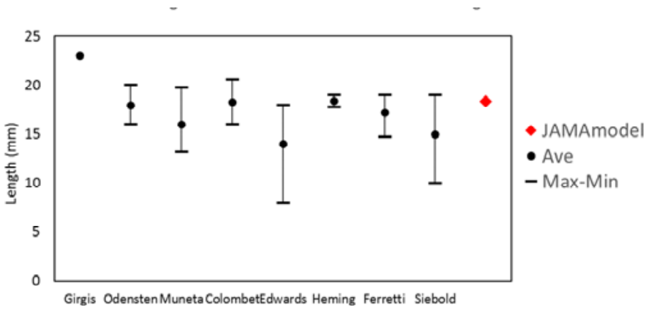

c) Length measurement of the ACL femoral origin

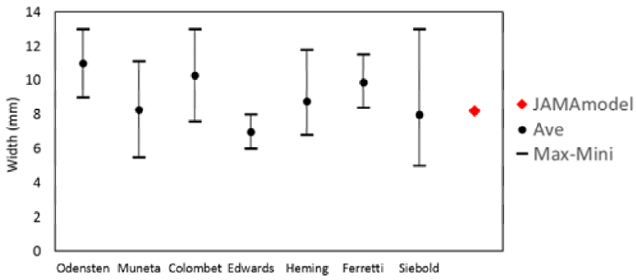

d) Width measurement of the ACL femoral origin

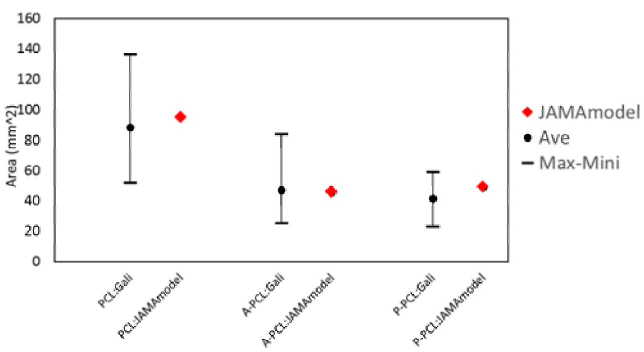

e) Area measurement of the PCL tibial insertion

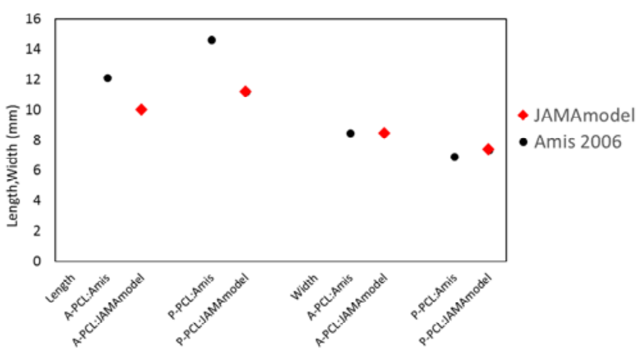

f) Length and Width measurement of the femoral PCL

Fig. A7. Comparison of the ACL and PCL attachment areas with experimental data [28-41].

TABLE AI Result of the injuries of the knee 4-point bending test [9]

PMHS ID	ACL	PCL	MCL	LCL
Bend 1	-	-	P	-
Bend 2	-	-	P	-
Bend 3	-	-	P	-
Bend 4	-	-	P	-
Bend 5	-	-	C	-
Bend 6	-	-	P	-
Bend 7	-	-	-	-
Bend 8	-	-	P	-
- : No injury, P: Partial avulsion, C: Complete avulsion				

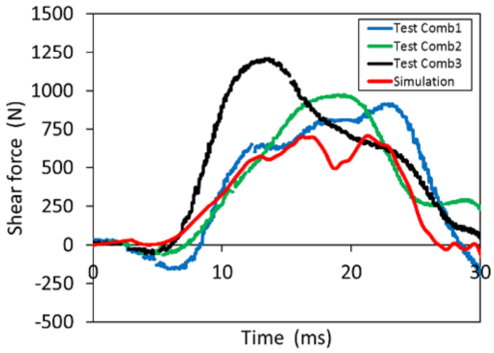

a) Comparison of moment-angle response for the knee 3-point bending test

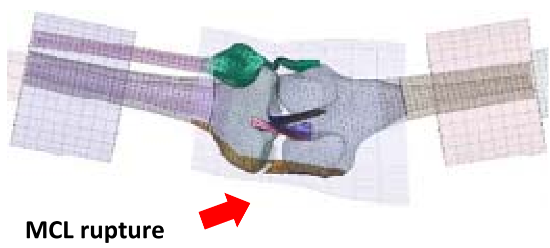

b) Comparison of moment-angle response for the knee 3-point bending test

Fig. A8. knee 3-point bending test [9].

TABLE AII Result of the injuries of the knee 3-point bending test [9]

PMHS ID	ACL	PCL	MCL	LCL
Comb 1	-	-	-	-
Comb 2	-	-	C	-
Comb 3	-	-	B	-
Comb 4	-	-	C	-
Comb 5	L	-	C	-
Comb 6	-	-	P	-
Comb 7	-	-	P	-
Comb 8	-	-	P	-
- : No injury, P: Partial avulsion, C: Complete avulsion B: Bony Avulsion, L: Slight laxity				

Pelvis model validation result

TABLE AIII Results of the injuries of pelvis dynamic loading impact tests (Acetabulum impact) [10]

PMHS ID	Injury pattern
1.5	R: fx PR, fx SIJ along the sacral holes
1.6	R: fx PR, fx along the SH, L: fx PR
1.7	R: fx PR, fx Sacrum ala
1.8	R: Complex fx of the acetabulum, fx PR
1.9	R: Complex fx of PR and PS, fx along the SH
1.10	R: fx PR, Complex fx of SH and SIJ
SH: sacral holes, PR: pubic ramus/rami, PS: pubic symphysis, SIJ: sacroiliac joint, fx: fracture	

TABLE AIV Results of the injuries of pelvis dynamic loading impact tests (Iliac impact) [10]

PMHS ID	Injury pattern
1.11	disruption of PS, R: Partial dislocation of SIJ
1.12	PS Slight laxity, R: Slight laxity of SIJ
1.13	Tear PS, R: fx PR, fx SIJ
1.14	PS Slight laxity, R: dislocation of SIJ
1.15	R: fx Sacrum ala
1.16	Disruption of PS, R: Partial dislocation of SIJ
SH: sacral holes, PR: pubic ramus/rami, PS: pubic symphysis, SIJ: sacroiliac joint, fx: fracture	

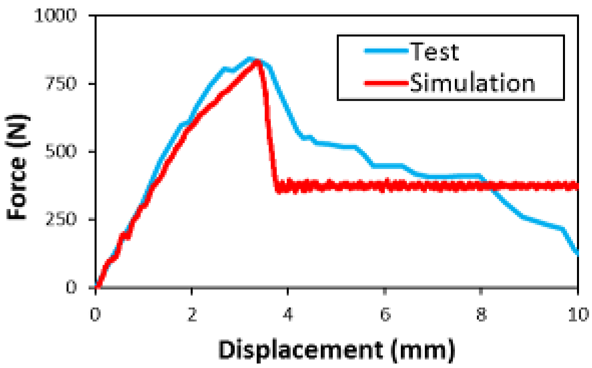

a) Tension test result

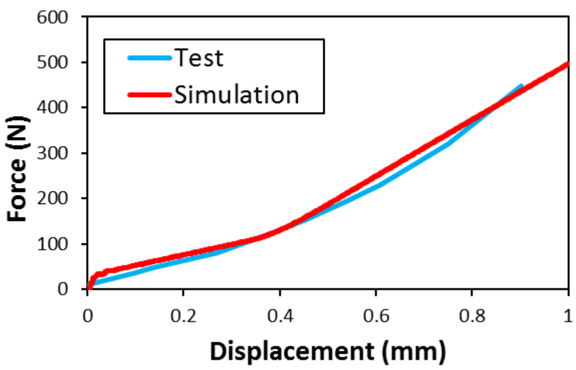

b) Compression test result

Fig. A9. Pubic symphysis compression and tension tests [46].

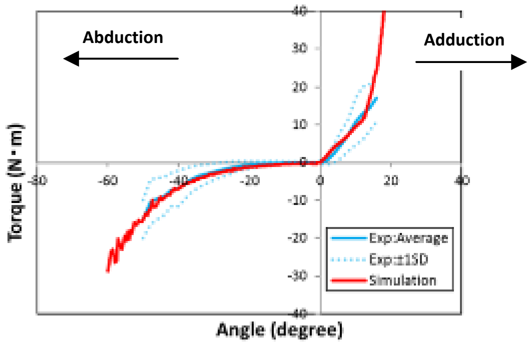

Fig. A10. Comparison of torque-angle response for the hip joint adduction and abduction test [47].

Generic buck component model validation result

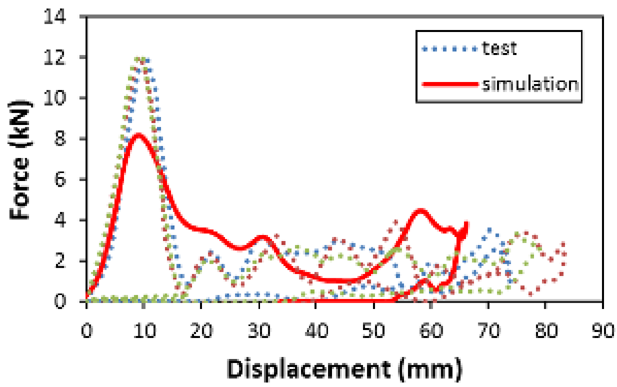

a) Comparison of moment-angle response for hood impact test

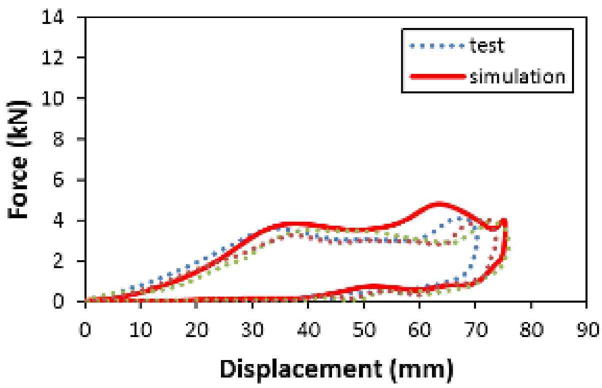

b) Comparison of moment-angle response for the grille impact test

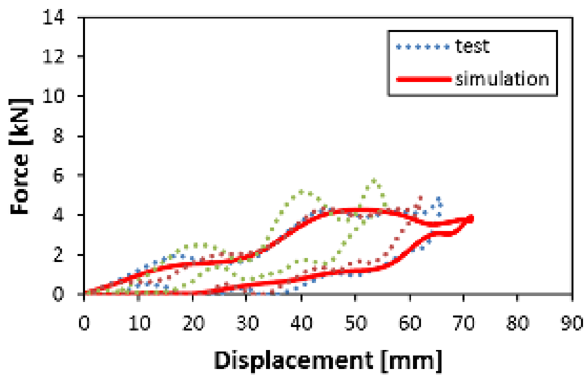

c) Comparison of moment-angle response for the bumper impact test
Fig. A11. Generic buck component model validation test [16].

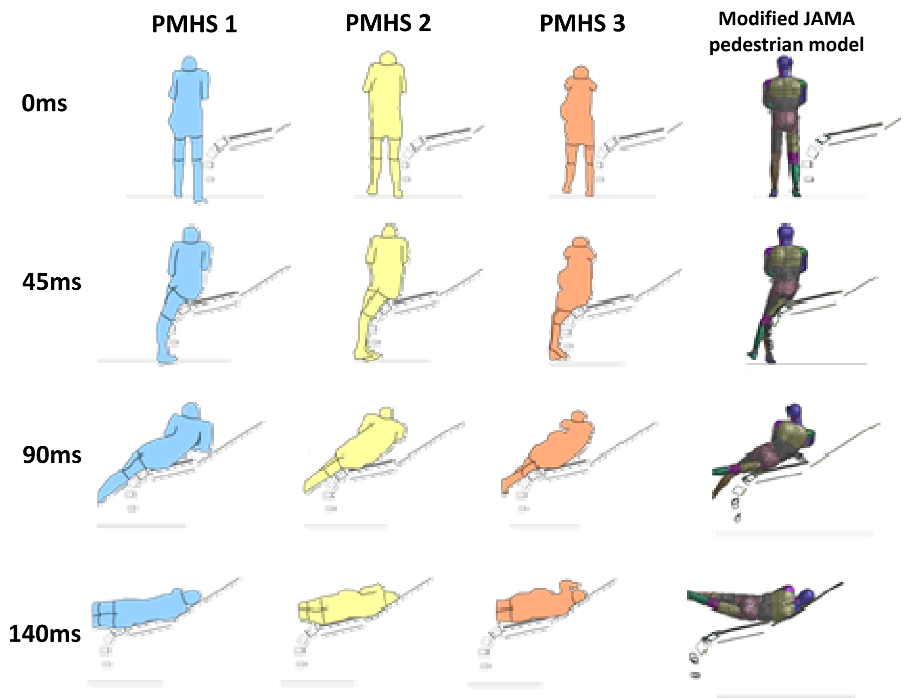

Fig. A12. Comparison of whole-body kinematics (side view) of PMHS tests and simulation results [15].

VIII. APPENDIX B

Thigh and leg model properties

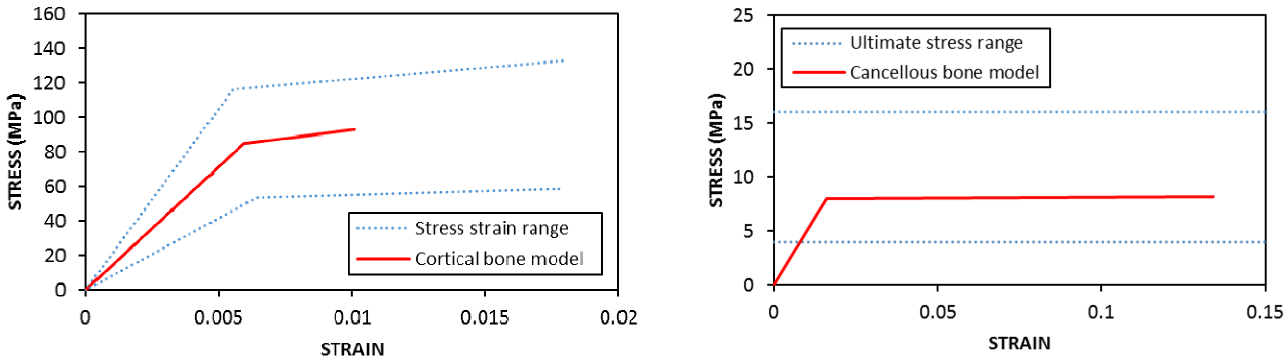

a) Cortical bone model material property [79] b) Cancellous bone model material property [59-61]

Fig. B1. Quasi-static stress-strain curve for cortical and cancellous bone of leg.

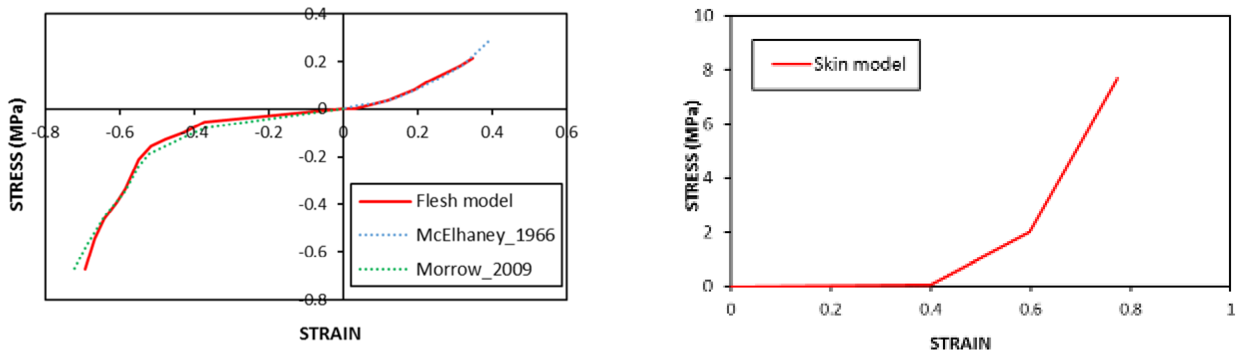

a) Flesh model material property [64-65] b) Skin model material property [80-81]

Fig. B2. Quasi-static stress-strain curve for flesh and skin of leg.

Knee model properties

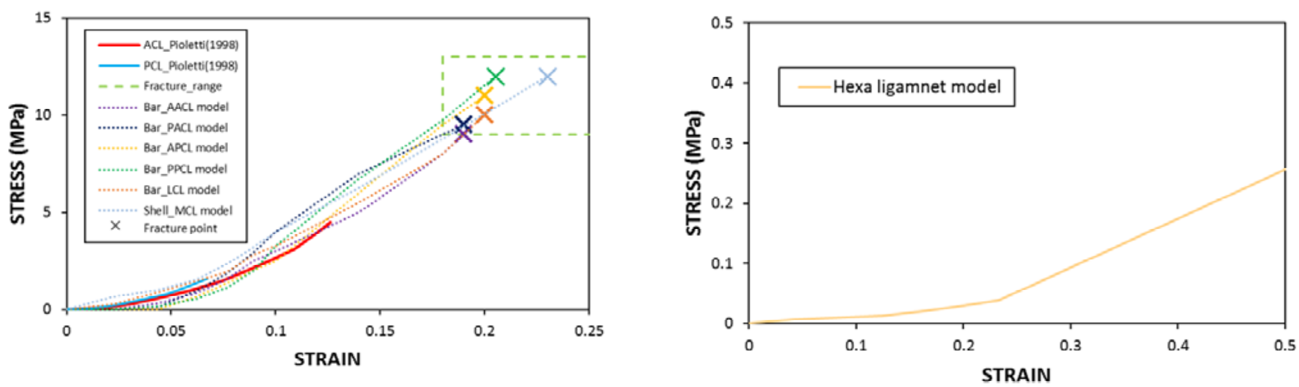

a) Knee ligament bar model material property [50-54] b) Knee ligament hexa model material property

Fig. B3. Quasi-static stress-strain curve for knee ligaments.

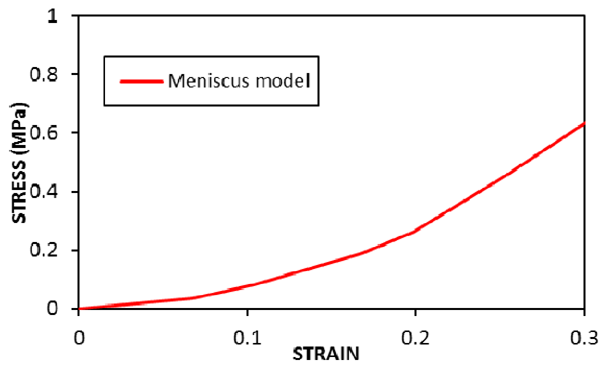

Fig. B4. Stress-strain curve for the meniscus model [55].

Pelvis model properties

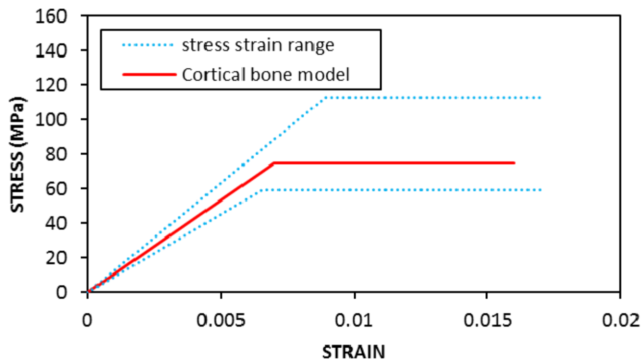

a) Cortical bone model material property [10][58]

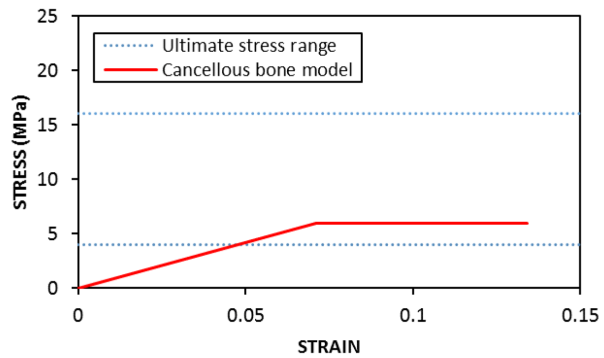

b) Cancellous bone model material property [59-61]

Fig. B5. Quasi-static stress-strain curve for cortical and cancellous bone of pelvis.

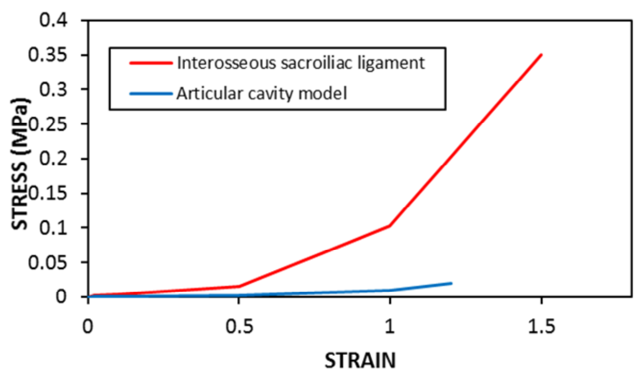

Fig. B6. Quasi-static stress-strain curve for sacroiliac ligament[10].

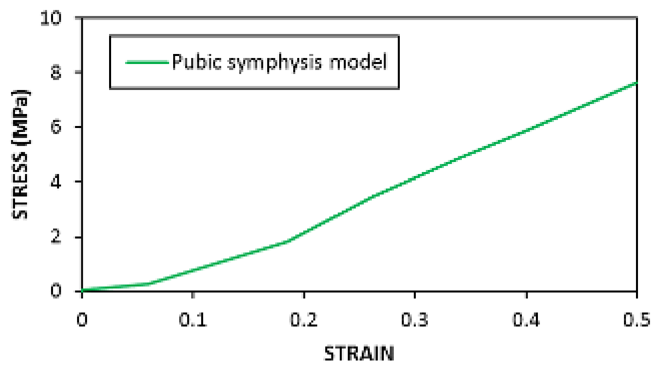

a) Pubic symphysis model material property of compression [46]

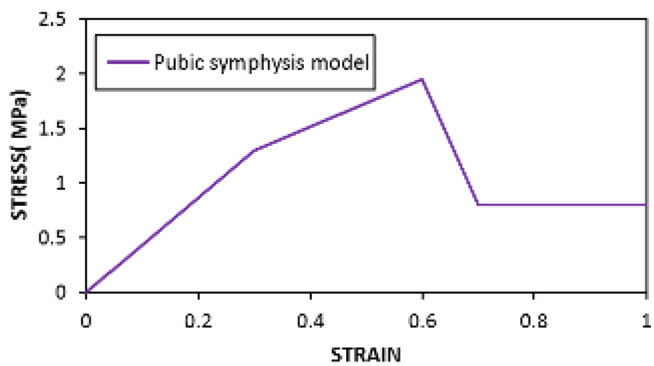

b) Pubic symphysis model material property of tension [46]

Fig. B7. Quasi-static stress-strain curve for pubic symphysis.

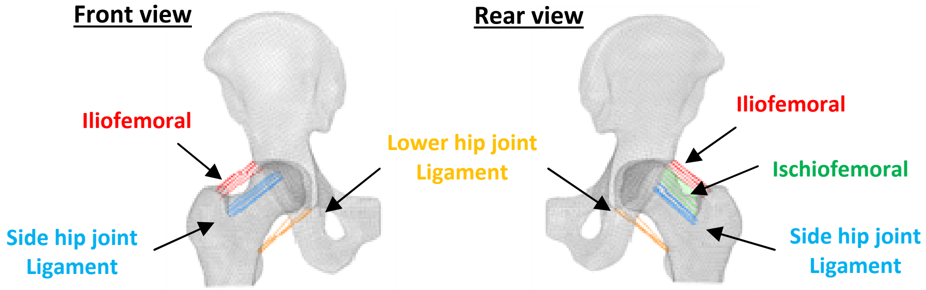

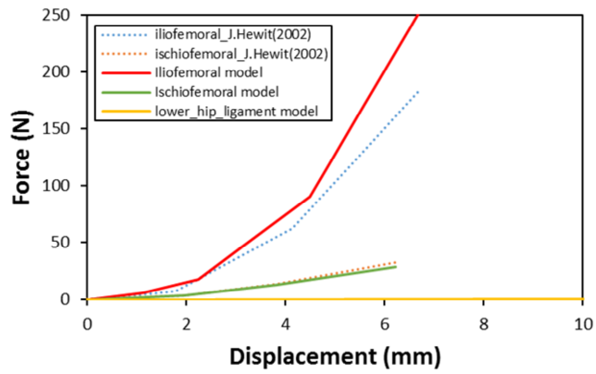

a) Hip joint model material property of tension (small deformation) [82-84]

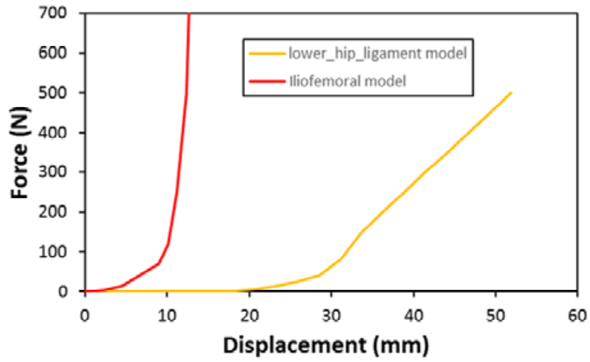

b) Hip joint model material property of tension (large deformation) [82-84]

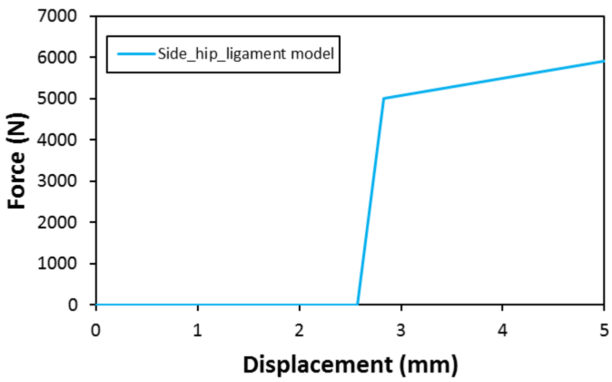

c) Side hip joint model material property [47]

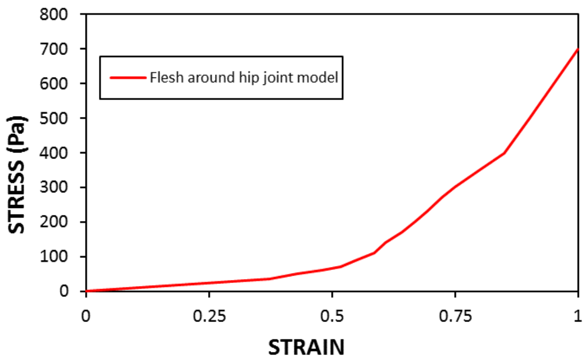

d) Flesh around hip joint model material property [47]

Fig. B8. Quasi-static stress-strain curve for hip joint.